photonics

MDPI

Review

Integrated Components and Solutions for High-Speed Short-Reach Data Transmission

Lin Jiang [1], Lianshan Yan [1,*], Anlin Yi [1], Yan Pan [1], Bo Zhang [2], Qianggao Hu [2], Wei Pan [1] and Bin Luo [1]

[1] Center for Information Photonics & Communications, School of Information Science and Technology, Southwest Jiaotong University, Chengdu 611756, China; linjiang@swjtu.edu.cn (L.J.); anlinyi@swjtu.edu.cn (A.Y.); py_swjtu@foxmail.com (Y.P.); wpan@home.swjtu.edu.cn (W.P.); bluo@swjtu.edu.cn (B.L.)

[2] Accelink Technologies Co., Ltd., Wuhan 430205, China; bo.zhang@accelink.com (B.Z.); qianggao.hu@accelink.com (Q.H.)

* Correspondence: lsyan@swjtu.edu.cn

Abstract: According to different transmission distances, application scenarios of a data center mainly include intra- and inter-data center optical interconnects. The intra-data center optical interconnect is considered as a few kilometers optical interconnect between servers and racks inside a data center, which accounts for nearly 80% of data traffic of a data center. The other one, inter-data center optical interconnect, is mainly applied in tens of kilometers data transmission among different data centers. Since data exchange in data centers generally occurs between many servers and racks, and a lot of transmitter and receiver components are required, optical interconnects become highly sensitive to component costs. In this paper, we firstly review the development and applications of mainstream transmitter components (e.g., VCSEL, DML, EML, MZM, and monolithic integrated transmitter) and receiver components (e.g., single-end photodetector, Kramers-Kronig receiver, Stokes vector receiver, and monolithic integrated receiver), which have been widely applied in short-reach transmission systems. Then, two types of integrated solutions including simplified detection scheme and transceiver integration scheme are presented in detail. Finally, we summarize and discuss the technological and component options for different transmission distances. We believe that monolithic integrated components, especially transceiver integration, will become a powerful solution for next-generation high-speed short-reach transmission systems.

Keywords: short-reach transmission link; direct detection; coherent detection; transceiver; Kramers-Kronig receiver; Stokes vector receiver; monolithic integrated components

Citation: Jiang, L.; Yan, L.; Yi, A.; Pan, Y.; Zhang, B.; Hu, Q.; Pan, W.; Luo, B. Integrated Components and Solutions for High-Speed Short-Reach Data Transmission. *Photonics* **2021**, *8*, 77. https://doi.org/10.3390/photonics8030077

Received: 31 January 2021
Accepted: 12 March 2021
Published: 14 March 2021

1. Introduction

In recent years, with the applications of various multimedia and data services (e.g., Internet of Things, cloud computing, remote surgery, the construction of 5G, and beyond 5G networks), global network traffic has presented explosive growth over the past decade [1]. Since massive data needs to be stored, transmitted, and processed in a data center, the corresponding traffic also grows rapidly. As the intra- and inter-data center optical interconnects in data center application scenarios [2] require a large number of transmitter and receiver components between servers and racks, the component cost plays a critical role in optical interconnects [3].

Even though the coherent solution with IQ modulation and coherent detection beyond 100-Gbit/s is relatively mature, its transmitter and receiver components with high cost and large footprint size cannot be directly transplanted to short-reach transmission systems. Considering the cost and footprint size, 100-Gbit/s short-reach transmission systems prefer intensity modulation and direct detection (IM/DD) technology [4]. In recent years, numerous 100-Gbit/s IM/DD-based solutions with different transmitter and receiver components have been demonstrated. In these solutions, the transmitter components mainly are

vertical-cavity surface-emitting laser (VCSEL) [5–7], directly modulated laser (DML) [8,9], Mach-Zehnder modulator (MZM) [10,11], integrated electro-absorption modulated laser (EML) [12–14], and monolithic integrated transmitter [15,16]. The receiver components usually contain single-end photodetector (PD), Kramers-Kronig receiver [17,18], Stokes vector receiver [19–21], and monolithic integrated receiver [22,23]. Here, it is commonly considered that monolithic integrated transmitter and receiver under low-cost and small footprint size have great potential to be the candidate transmitter and receiver component for next-generation high-speed short-reach transmission systems.

In order to further increase the transmission capacity of IM/DD systems, advanced multi-level modulation formats, polarization division multiplexing, and powerful digital signal processing algorithms have been introduced to support high-speed short-reach transmission systems [24]. However, when a lane rate increases from 100-Gbit/s to 400-Gbit/s, a smooth transition from the IM/DD technology to digital coherent technology will be in progress; of course, there are still many challenges. The conventional transmitter and receiver components in digital coherent technology are not cost-effective [25], so that these components cannot be directly transplanted to short-reach transmission systems. In addition to the digital coherent technology and the traditional IM/DD technology, some advanced direct detection technologies such as Kramers-Kronig receiver [17,18] and Stokes vector receiver [19–21] have been proposed and studied extensively. Since these techniques can reconstruct the complex domain of the signal, rate-distance product can be further improved by combing impairments compensation algorithms and advanced modulation technology. These advanced techniques can be treated as a compromise between the digital coherent technology and the traditional IM/DD technology. Recently, an effective solution, a transceiver integration scheme based on the digital coherent technology [26,27], has been reported and shows the potential to reduce cost and footprint size of the transmitter and receiver components dramatically. Subsequently, the transceiver integration scheme for multiple parallel IM/DD channels [28] has also been demonstrated.

The rest of this paper is organized as follows. We firstly review mainstream transmitter components (e.g., VCSEL/DML/EML/MZM/monolithic integrated transmitter) in Section 2, and then review mainstream receiver components (e.g., single-end PD /Kramers-Kronig receiver/Stokes vector receiver/monolithic integrated receiver) in Section 3. Next, Section 4 describes a simplified detection scheme and two transceiver integration schemes under direct and coherent detections. In Section 5, the technological and component options for different transmission distances are discussed. Finally, our conclusions and outlook are summarized in Section 6.

2. Transmitter for Short-Reach Transmission Systems

Unlike long-haul transmission systems that prefer to use expensive IQ modulators to obtain high-speed transmission rate, short-reach transmission systems are very sensitive to component cost because these systems are often used in a data center, enabling data exchange between many servers and racks [3]. Thus, low-cost IM/DD technology has been firstly considered for 100-Gbit/s short-reach transmission systems. In this section, we review recent applications of the five types of transmitters (e.g., VCSEL, DML, EML, MZM, and monolithic integrated transmitter) in IM/DD systems.

2.1. Vertical-Cavity Surface-Emitting Laser

Multimode (MM) VCSEL together with multimode fiber (MMF) have been widely used in short-reach optical interconnects, especially in transmission distances less than 300 m [24,29]. For MM-VCSEL, a record 3-dB modulation bandwidth of 30-GHz had been reported with low threshold current and high energy efficiency [30]. As shown in Figure 1a, the MM-VCSEL started to work when the voltage exceeded 1.5-V and the threshold current reached 0.25-mA. The optical spectrum at a bias current of 2-mA was inserted in Figure 1a. The small-signal modulation responses at different bias currents (e.g., 1-mA, 1.3-mA, 2-mA, and 4.1-mA) were depicted in Figure 1b. The measured modulation response at a bias current of 4.1-mA can

reach the highest bandwidth 30-GHz ever reported. Owing to the small oxide aperture of the MM-VCSEL, the resonance frequency f_r increased rapidly with the square root of current I_b-I_{th} at a rate of 17.5-GHz/mA$^{1/2}$, reaching a maximum value of 27-GHz, as shown in the illustration of Figure 1b. Similarly, 3-dB modulation bandwidth f_{3dB} increased rapidly with the square root of current I_b-I_{th} at a rate of 20.6-GHz/mA$^{1/2}$, reaching a value of 25 GHz already at 1.8-mA. In here, *D*-factor was defined as a rate factor consisting of resonance frequency f_r and square root of current I_b-I_{th}. MCEF was the modulation current efficiency factor, which was a rate factor consisting of 3-dB bandwidth f_{3dB} and square root of current I_b-I_{th}. At present, various beyond 100-Gbit/s MM-VCSEL-based short-reach transmission solutions have been reported [31–45]. R. Puerta et al. demonstrated 107.5-Gbit/s MultiCAP short-reach transmission over 10-m OM4 MMF [31]. S. A. Gebrewold et al. reported on the transmission of 108-Gbit/s PAM-8 signal over 25-m OM3 MMF [32]. J. Lavrencik et al. utilized an unpackaged MM-VCSEL to realize beyond 168-Gbit/s PAM-4 data transmission over 50-m OM5 [35]. Subsequently, T. Zuo et al. experimentally demonstrated 112-Gbit/s duobinary PAM-4 short-reach optical interconnects with a 200-m MMF link [36], and then the transmission rate was further increased to 200-Gbit/s [37]. For these schemes, mode dispersion resulting in severe inter-symbol interference (ISI) was considered to be the main limiting factor in terms of high-speed transmission rate and long-haul transmission distance. Here, one effective solution was to apply single-mode (SM) VCSEL to reduce the number of transverse modes. Compared to the MM-VCSEL-based systems, the SM-VCSEL combining MMF and single-mode fiber (SMF) can improve system performance and support more than a few kilometers transmission reach [39–45]. In addition, since the light direction of VCSEL laser output is perpendicular to the substrate, it is particularly convenient for array integration (i.e. multiple VCSEL lasers can be arranged in parallel in the direction perpendicular to the substrate). Here, the recent applications of SM-/MM-VCSEL in beyond 100-Gbit/s per lane data transmission are summarized in Table 1.

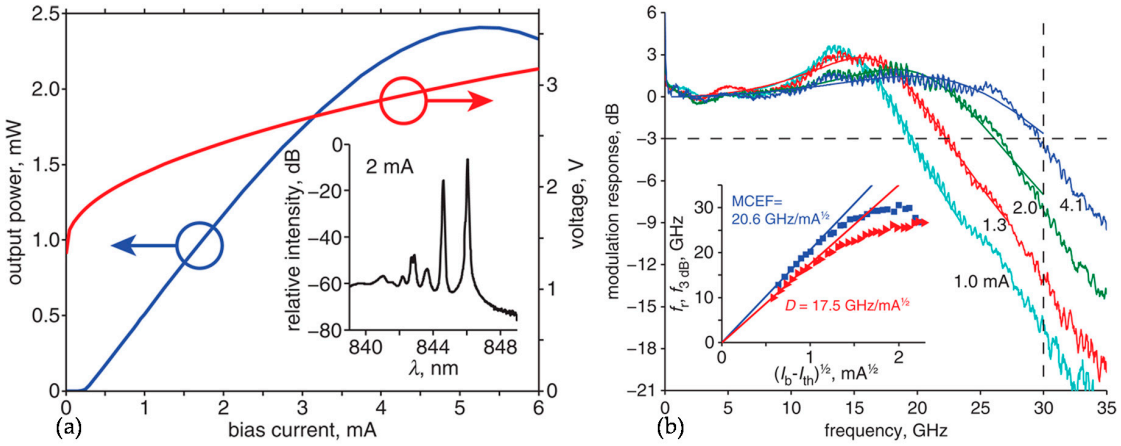

Figure 1. (**a**) Light-current-voltage characteristics (Inset: optical spectrum at a bias current of 2-mA); (**b**) small-signal modulation responses at bias currents of 1-mA, 1.3-mA, 2-mA, and 4.1-mA (Inset: resonance frequency f_r and 3-dB bandwidth f_{3dB} of VCSEL plotted against square root of bias current I_b above threshold I_{th}); I_b: bias current; I_{th}: threshold current; *D*-factor: a rate factor consisting of resonance frequency f_r and square root of current I_b-I_{th}; MCEF: the modulation current efficiency factor; (From [30], © 2015 IEEE).

Table 1. Incomplete summary of SM-/MM-VCSEL applied in beyond 100-Gbit/s per lane data transmission.

Tx Device	λ (nm)	MF	BW (GHz)	Rate (Gbit/s)	Reach (m)	Fiber Type	FEC Limit	Ref.
MM-VCSEL	850	MultiCAP	~20	107.5	10	OM4-MMF	3.8×10^{-3}	[31]
MM-VCSEL	850	PAM-8	–	108	25	OM3-MMF	3.8×10^{-3}	[32]
MM-VCSEL	850	MultiCAP	25	112	150	OM4-MMF	3.8×10^{-3}	[33]

Table 1. *Cont.*

Tx Device	λ (nm)	MF	BW (GHz)	Rate (Gbit/s)	Reach (m)	Fiber Type	FEC Limit	Ref.
MM-VCSEL	850	PAM-4	22	112	200	OM4-MMF	2×10^{-4}	[34]
MM-VCSEL	850	PAM-4	~28	168	50	OM5-MMF	$>1 \times 10^{-6}$	[35]
MM-VCSEL	850	PAM-4	25	112	200	OM4-MMF	4.2×10^{-4}	[36]
MM-VCSEL	850	PAM-4	25	200	100	OM4-MMF	4×10^{-3}	[37]
MM-VCSEL	850	PAM-4	20	100	100	OM3-MMF	3.8×10^{-3}	[38]
SM-VCSEL	850	DMT	26	161	10	OM4-MMF	2.7×10^{-2}	[39]
SM-VCSEL	850	DMT	25	112	300	OM4-MMF	3.8×10^{-3}	[40]
SM-VCSEL	1543	PAM-4	~23	100	1000	SMF	3.8×10^{-3}	[41]
SM-VCSEL	1543.2	PAM-4	22	100	2500	SMF	3.8×10^{-3}	[42]

2.2. Directly Modulated Laser

At transmitter side of short-reach transmission systems, another low-cost light source, DML with high output power and small footprint size, is more desirable than other externally modulated components. In recent years, in order to support 100-Gbit/s even beyond 100-Gbit/s transmission systems, the modulation bandwidth of DML is required to increase from commercial 10-GHz to higher bandwidth. Here, an advanced modulation bandwidth of 55-GHz was developed using photon-photon resonance and detuned-loading effects, and it is demonstrated in 112-Gbit/s PAM-4 system [46]. As shown in Figure 2a, the normalized S_{21} amplitude modulation responses for the bias range from 10-mA to 36.2-mA at 25 °C were measured, and the 3-dB bandwidth of 55-GHz was obtained at 36.2-mA bias condition. The peak of the normalized S_{21} amplitude modulation response can be observed around 50-GHz. In addition, a wider frequency modulation bandwidth about 65-GHz was depicted in Figure 2b, which can prove that the DML can work in such high frequency modulation. Thanks to the photon-photon resonance, the bandwidth can be further boosted beyond 100-GHz for a membrane short-cavity DR laser on a SiC substrate [47]. Nowadays, there are a variety of DML-based high-speed data transmission schemes reported in C- or O-band transmission systems. D. Li et al. experimentally demonstrated 4 × 96-Gbit/s PAM-8 transmission over 15-km SMF by using four O-band DMLs (1269.54-nm, 1290.10-nm, 1309.67-nm, and 1329.12-nm) with the narrowest 3-dB bandwidth of 13.5-GHz [48]. Z. Xu et al. utilized a 16-GHz C-band DML to realize 100-Gbit/s PAM-4 short-reach data transmission over 15-km SMF with only post-equalization [9]. Also based on O-band DML, W. Yan et al. demonstrated 117-Gbit/s DMT over 40-km and 101-Gbit/s DMT over 80-km transmissions [49]. Y. Gao et al. applied 28-GHz O-band DML to achieve 112-Gbit/s single-carrier, single-polarization PAM-4 short-reach transmission [50]. Furthermore, W. Wang, et al. proposed a simple and cost-effective packaging compensation method to enhance the resonance of the DML module at high frequency so that transmission distance can be increased to 40-km [8]. Recently, beyond 200-Gbit/s, DML-based data transmission schemes also had been widely reported [47,51–53]. S. Yamaoka et al. reported a line rate of 256-Gbit/s PAM-4 transmission over 2-km SMF based on beyond 100-GHz DML laser [47], and this group further demonstrated 325-Gbit/s and 321.24-Gbit/s at back-to-back (BTB) and after 2-km SMF link [51]. D. Che et al. designed a short-cavity 54-GHz O-band DBR laser integrated with a short semiconductor optical amplifier (SOA) section, and demonstrated a line rate of 240-Gbit/s PAM-8 transmission over 10-km SMF link [52]. Recently, a fast data transmission of line rate 368.8-Gbit/s over 15-km SMF in the O-band was demonstrated [53]. Here, the recent applications of DML in beyond 100-Gbit/s per lane data transmission are summarized in Table 2. Besides intensity modulation, some groups had been exploring to utilize modulation-dependent frequency chirp of DML to generate phase modulation alone with the intensity for further improving transmission capacity [54,55]. In conclusion, we believe that DML has great potential to be used in 100-Gbit/s or even higher speed short-reach transmission systems with a few to tens of kilometers transmission distance.

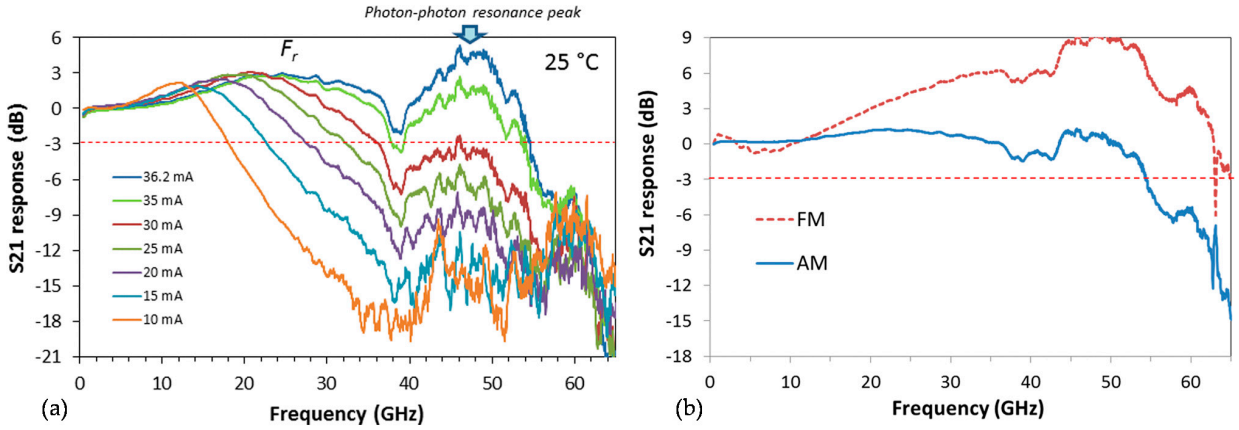

Figure 2. (**a**) S_{21} amplitude responses for a bias range from 10–36.2 mA at 25°C; (**b**) S_{21} amplitude and frequency responses at 36.2 mA gain bias at 25°C; FM: Frequency modulation; AM: Amplitude modulation; (From [46], © 2017 IEEE).

Table 2. Incomplete summary of DML applied in beyond 100-Gbit/s per lane data transmission.

Tx Device	λ (nm)	MF	BW (GHz)	Rate (Gbit/s)	Reach (km)	Fiber Type	FEC Limit	Ref.
DML	1310	PAM-4	28	112	40	SMF	3.8×10^{-3}	[8]
DML	C-band	PAM-4	16	100	15	SMF	3.8×10^{-3}	[9]
DML	1300	PAM-4	55	112	2.2	SMF	2×10^{-4}	[46]
DML	1310	DMT	18	117	40	SMF	1×10^{-3}	[49]
DML	1308.45	PAM-4	25	112	20	SMF	4.6×10^{-3}	[50]
DML	1286	PAM-4	>100	256	2	SMF	3.8×10^{-3}	[47]
DML	1295.48	DMT	104.5	321.24	2	SMF	3.8×10^{-3}	[51]
DML	1315	PAM-8	54	240	10	SMF	1.8×10^{-2}	[52]
DML	1313	DMT	65	368.8	15	SMF	1.8×10^{-2}	[53]

2.3. $LiNbO_3$ Mach-Zehnder Modulator

In the early development of direct modulation components, bandwidth limitation may be the main obstacle to realize high-speed transmission rate. The external modulation component, $LiNbO_3$ MZM modulator, has been extensively reported in 100-Gbit/s and beyond 100-Gbit/s short-reach transmission systems [56–60]. P. Gou et al. applied artificial neural networks as signal equalization technology to realize 120-Gbit/s PAM-8 10-km transmission [56]. L. Zhang et al. achieved beyond 100-Gbit/s single-sideband (SSB) DMT transmission over 80-km SMF assisted by dual-drive (DD) MZM [57]. H. Mardoyan et al. demonstrated 168-Gbit/s PAM-4 generation and C-band 1-km transmission [58]. Moreover, based on Tomlinson-Harashima precoding, Q. Hu et al. reported 168-Gbit/s PAM-4 transmission over 2-km SMF with 33-GHz brick-wall bandwidth limitation [59]. To extend transmission distance, Q. Zhang et al. used a DDMZM to generate chromatic dispersion (CD) pre-compensated signal and achieve 128-Gbit/s 80-km transmission [60]. Recently, various beyond 200-Gbit/s transmission schemes have been demonstrated as listed later [61–67]. S. Yamamoto et al. proposed a simple nonlinear trellis-coed-modulation scheme to realize spectral shaping for a 255-Gbit/s PAM-8 transmissions system over 10-km SMF under 20-GHz component bandwidth limitation without any optical amplifier [61]. F. Buchali et al. presented 200-Gbit/s PAM4 40-km dispersion management transmission with 14-GHz analog to digital converter (ADC) bandwidth [62]. Furthermore, probability shaping modulation format was also introduced to achieve better transmission performance. J. Zhang et al. reported single-lane 280-Gbit/s PS-PAM-8 transmission over 10-km SMF link based on pre-equalization and clipping technique [67]. The recent applications of MZM under beyond 100-Gbit/s per lane have been summarized as shown in Table 3. As mentioned above, $LiNbO_3$ MZM modulator with a large modulation bandwidth and no frequency chirp effect had been widely applied in various beyond 100-Gbit/s short-

reach transmission systems, but the component cost and power consumption were still considered as the limiting factors. In recent years, combining the advantages of $LiNbO_3$ MZM modulator, some groups are exploring various integrated MZM solutions to reduce footprint size, power consumption, and cost to meet the demands of low-cost and power-efficient short-reach transmission systems under tens of kilometers transmission distance.

Table 3. Incomplete summary of MZM applied in beyond 100-Gbit/s per lane data transmission.

Tx Device	λ (nm)	MF	BW (GHz)	Rate (Gbit/s)	Reach (km)	Fiber Type	FEC Limit	Ref.
MZM	1550	PAM-8	30	120	10	SMF	1×10^{-2}	[56]
DDMZM	1550	DMT	22	105	80	SMF	4.5×10^{-3}	[57]
MZM	1545	PAM-4	40	168	1	SMF	3.8×10^{-3}	[58]
MZM	1550	PAM-4	33	168	2	SMF	3.8×10^{-3}	[59]
DDMZM	~1555	PAM-4	30	128	80	SMF	2.4×10^{-2}	[60]
MZM	1304.6	PAM-8	30	255	10	SMF	2.5×10^{-4}	[61]
MZM	1550	PAM-4	40	200	40	SMF + DCF	3×10^{-4}	[62]
MZM	C-band	DMT	30	244	1	SMF	4.5×10^{-3}	[63]
DDMZM	O-band	PAM-8	30	240	2	MCF	3.8×10^{-3}	[65]
MZM	1293	PAM-6	28	225	2	SMF	3.8×10^{-3}	[66]
MZM	1310.96	PS-PAM-8	60	280	10	SMF	3.8×10^{-3}	[67]

2.4. Electro-Absorption Modulated Laser

An EML, which monolithically integrates a distributed feedback laser and an electro-absorption modulator on one chip, has been studied and applied in short-reach transmission systems. EML takes the advantages of DFB laser and the excellent modulation property of an external modulator. Therefore, EML can offer higher tolerance to CD and present lower frequency chirp compared with DML. Based on the above advantages, the EML-based systems can achieve higher transmission rate and longer transmission distance than DML-based systems. Meanwhile, EML may present smaller footprint size, lower power consumption, and lower cost than that of MZM. The application of EML had been demonstrated in various beyond 100-Gbit/s verification experiments [68–78]. K. Wang et al. utilized an 18-GHz O-band EML to realize 100-Gbit/s PAM-4 signal transmission over an 80-km SMF link [68]. In addition, K. Zhong et al. demonstrated an amplifier-less transmission of a single lane 112-Gbit/s PAM-4 signal over 40-km SMF using 25-GHz O-band EML at 7% HD-FEC threshold of 3.8×10^{-3} [70]. C. Chuang et al. designed a novel convolutional neural network-based nonlinear classifier to achieve lower bit error rate (BER) performance 3.5×10^{-6} under the same bitrate and distance [71]. Furthermore, W. Wang et al. experimentally presented a single-wavelength single-polarization 35-GHz-class commercial EML-based 214-Gbit/s PAM-4 signal transmission [74]. Based on pre-equalization and clipping technique, J. Zhang et al. reported a single-lane C-band EML-based 260-Gbit/s PS-PAM-8 signal transmission over 1-km NZDSF link [75]. In order to achieve higher transmission rate, researchers further explored to enhance the bandwidth of EML. Until now, the EML monolithically integrating a distributed feedback laser and a traveling-wave electro-absorption modulator (DFB-TWEAM) was reported as the maximum bandwidth of 100 GHz [13]. Figure 3a illustrated the DFB-TWEAM and biasing schema. The small signal modulation responses (electrical reflection S_{11} and electro-optic S_{21}) of DFB-TWEAM were measured as shown in Figure 3b,c. It can be observed that the 3-dB bandwidth was greater than 100-GHz. The applications about the monolithically integrated C-band DFB-TWEAM have been reported in 204-Gbit/s OOK [76], 200-Gbit/s PAM-4 [77], and 200-Gbit/s DMT [78] transmission systems. The recent applications of EML in beyond 100-Gbit/s per lane data transmission have been summarized as shown in Table 4. These results denote that EMLs would have great potential to be used in low-cost and energy-efficient beyond 100-Gbit/s short-to-medium reach transmission systems,

and may be a potential candidate for the next-generation 400-Gbit/s, even 800-Gbit/s data transmission systems.

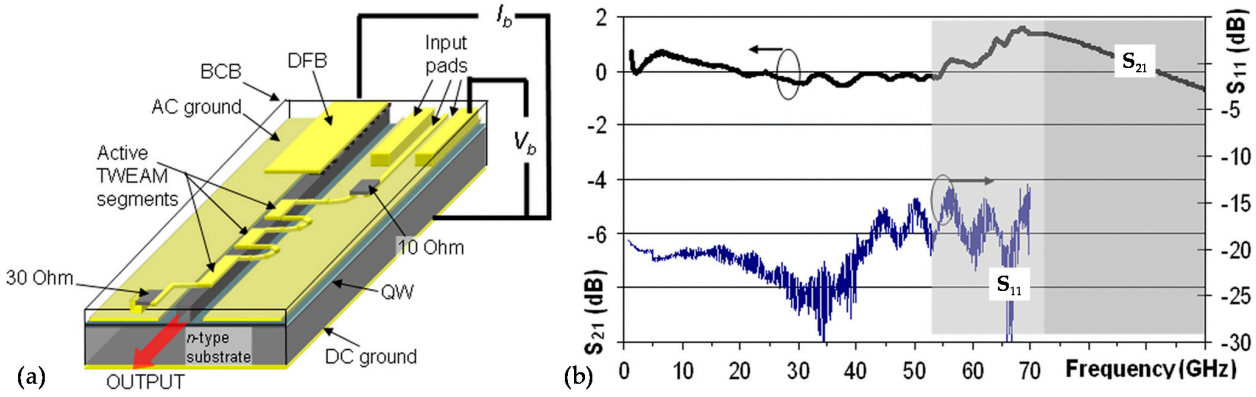

Figure 3. (**a**) Schema of DFB-TWEAM; (**b**) S_{21} and S_{11} characteristics of TWEAM; DFB: distributed feedback laser; TWEAM: traveling-wave electro-absorption modulators; QW: quantum wells; BCB: BenzoCycloButene layer; AC: alternating current; DC: direct current; (From [13], © 2009 IEEE).

Table 4. Incomplete summary of EML applied in beyond 100-Gbit/s per lane data transmission.

Tx Device	λ (nm)	MF	BW (GHz)	Rate (Gbit/s)	Reach (km)	Fiber Type	FEC Limit	Ref.
EML	1298.5	PAM-4	18	100	80	SMF	3.8×10^{-3}	[68]
AXEL	~1307	PAM-4	35	106	60	SMF	2×10^{-4}	[69]
EML	1294.72	PAM-4	20	112	40	SMF	3.8×10^{-3}	[70]
EML	1293	PAM-4	25	112	40	SMF	3.5×10^{-6}	[71]
EML	1304	PAM-4	17	112	40	SMF	3.8×10^{-3}	[72]
DS-EML	1538.74	PAM-8	40	129	5	SMF	3.8×10^{-3}	[73]
EML	1310	PAM-4	35	214	10	SMF	2×10^{-4}	[74]
EML	1550	PS-PAM-8	40	260	1	NZDSF	2×10^{-2}	[75]
DFB-TWEAM	1550	OOK	>100	204	10	SMF + DCF	1.1×10^{-2}	[76]
DFB-TWEAM	1550	PAM-4	>100	200	0.4	SMF	2×10^{-2}	[77]
DFB-TWEAM	1550	DMT	>100	200	1.6	SMF	2.7×10^{-2}	[78]

2.5. Monolithic Integrated Transmitter

Compared with other discrete transmitter components, a monolithic integrated transmitter with the characteristics of lower power consumption, smaller size, lower cost, and higher reliability has shown great potential in short-reach even in metro transmission systems. Currently, mainstream monolithic integration technologies can be divided into two categories, including InP-based monolithic integration and silicon photonics (SiP). In addition, the use of InP-based monolithic integration transmitter has been widely explored to achieve high-speed and power-efficient signal transmission. For example, S. Lange et al. firstly reported a record 3-dB bandwidth up to 54-GHz InP-based DFB-MZM transmitter [15], and this was demonstrated in the 100-Gbit/s NRZ, 200-Gbit/s PAM-4 and 300-Gbit/s PAM-8 transmission systems with 1-kilometer distance. In addition, H. Yamazaki et al. presented 333-Gbit/s DMT transmission enabled by an 80-GHz C-band InP-based MZM over 20-km dispersion-compensated link [16]. Another attractive candidate, SiP, has the advantages of compatibility with complementary metal-oxide-semiconductor (CMOS) technology with small size and low loss, although many have questioned the intrinsic bottlenecks of the platform regarding modulator bandwidth at present. Several high-speed SiP transmitters have been reported for beyond 100-Gbit/s optical interconnects [15,16,79–91]. M. Li et al. experimentally achieved single lane 112-Gbit/s PAM-4 transmission over 1-km, 2-km, and 10-km SMF links based on 3-dB electro-optical bandwidth of beyond 50-GHz silicon MZM [79]. Furthermore, based on SiP-based DD

traveling-wave (TW) MZM, F. Zhang et al. demonstrated ultra-high-speed optical interconnects with single-lane bit rates of 176-Gbit/s PAM-4 [81] and 200-Gbit/s PAM-6 [82] for 1-km SMF transmission. Furthermore, this group further reported high baud-rate and long-haul transmission with SSB-PAM-N signal [83,84]. To further generate high baud-rate PAM-4 signal in optical domain, multi-electrode MZM (ME-MZM) [85] has been studied and shown better transmission performance compared to a traditional single electrode TW-MZM [86] at O-band. In addition, H. Mardoyan et al. reported a net rate of 222-Gbit/s OOK signal transmission over 200-m SMF link assisted by a small plasmonic-organic hybrid (POH) MZM, while the design cannot be entirely fabricated in commercial SiP processes [87]. H. Zhang et al. reported the 1-km optical transmission of an 800-Gbit/s (4 × 200-Gbits) PAM-4 signal using a four-channel SiP modulator chip with 3-dB bandwidth of 40-GHz [88]. Figure 4a showed a micrograph of the chip-on-board SiP transmitter, which integrated a four-channel SiP MZM chip and a four-channel driver chip. As depicted in Figure 4b, the 3-dB modulation bandwidth of silicon photonics modulator of different channels (e.g., CH_1, CH_2, CH_3, and CH_4) can both reach about 60-GHz, while that of silicon photonics transmitter co-packaged with the driver would reduce to about 40-GHz as shown in Figure 4c. In addition, other SiP transmitters, such as silicon micro-ring modulator [89,90] and hybrid silicon electro-absorption modulator [91], have also been reported. Part of these reports about monolithic integrated transmitter applied in beyond 100-Gbit/s data transmission is summarized in Table 5.

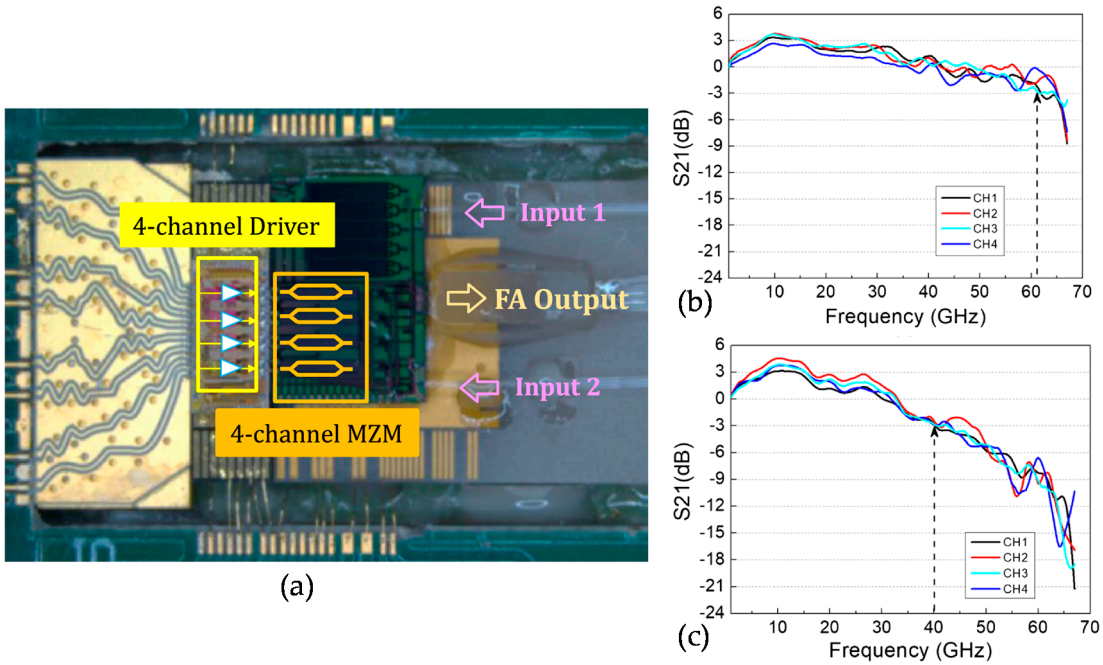

Figure 4. (**a**) Micrograph of the chip-on-board silicon photonics transmitter; (**b**) S_{21} characteristics of silicon photonics modulator under different channels (e.g., CH_1, CH_2, CH_3, and CH_4); (**c**) S_{21} characteristics of transmitter co-packaged with the driver under different channels. FA: fiber array; (From [88] © 2021 Chinese Laser Press).

Table 5. Incomplete summary of monolithic integrated transmitters applied in beyond 100-Gbit/s per lane data transmission.

Tx Device	λ (nm)	MF	BW (GHz)	Rate (Gbit/s)	Reach (km)	Fiber Type	FEC Limit	Ref.
InP-Based DFB-MZM	1542	PAM-8	54	300	1.2	SMF	1.9×10^{-2}	[15]
InP-Based MZM	1550	DMT	80	333	20	SMF + DCF	2.7×10^{-2}	[16]
SiP-based MZM	1550	PAM-4	>50	128	10	SMF + DCF	2×10^{-2}	[79]
SiP-based MZM	1310	PAM-8	20	112	10	SMF	3.8×10^{-3}	[80]

Table 5. *Cont.*

Tx Device	λ (nm)	MF	BW (GHz)	Rate (Gbit/s)	Reach (km)	Fiber Type	FEC Limit	Ref.
SiP-based DDTW-MZM	1546.98	PAM-4	22.5	176	1	SMF	1.5×10^{-2}	[81]
SiP-based DDTW-MZM	1546.98	PAM-6	22.5	200	1	SMF	1.5×10^{-2}	[82]
SiP-based DDTW-MZM	1546.98	SSB-PAM-4	22.5	176	400	SMF	4×10^{-2}	[83]
SiP-based DDTW-MZM	1546.98	PAM-4	22.5	184	320	SMF	2.4×10^{-2}	[84]
SiP-based ME-MZM	O-band	PAM-4	>35	112	10	SMF	2.4×10^{-2}	[85]
SiP-based TW-MZM	O-band	PAM-8	47	255	2	SMF	3.8×10^{-3}	[86]
SiP-based POH-MZM	1541.9	OOK	>70	222	0.12	SMF	2.24×10^{-2}	[87]
SiP-based 4ch-MZM	~1540	PAM-4	40	200	1	SMF	3.8×10^{-3}	[88]
SiP-based MRM	1541.57	PAM-4	47	160	1	SMF	2.12×10^{-3}	[89]

3. Receiver for Short-Reach Transmission Systems

It is well-known that short-reach transmission systems are mainly used in data center optical interconnects, access network, and metro network, etc. In such scenarios, the component costs need to be take into consideration as a variety of servers, switchers, and users are involved. Applying only one single-end PD in the system may greatly reduce cost and energy consumption, but it may not be able to meet ultra-high speed transmission systems because single-end PD only detects signal intensity. At present, some advance direct detection schemes, e.g., Kramers-Kronig receiver and Stokes vector receiver, have been proposed to improve the rate-distance product by combining impairments compensation algorithms with advanced modulation technology. Furthermore, monolithic integrated receivers with small footprint size, low power consumption, and low-cost have also been widely concerned and already demonstrated in various short-reach transmission systems. Next, we would review the recent applications of the four detection technologies.

3.1. Single-End Photodetector under Direct Detection

Single-end PD, which can perform the optoelectronic conversion operation to convert the signal from electrical domain to optical domain, is considered as the key receiver component of conventional IM/DD system. Single-end PD has been applied to detect signal envelope by square law detection. The output current of single-end PD is proportional to the square modulus of signal envelop, and hence it can only be used in amplitude modulation-based transmission systems. Usually, it is based on the reversely biased p-n junctions so that output current can be very weak. In order to enhance output current and receiver responsibility, two types of single-end PD including the PIN photodiode and the avalanche photodiode (APD) are introduced. The PIN photodiode consists of the p-type layer, intrinsic layer, and n-type layer, and normally combines with a trans-impedance amplifier (TIA) to further amplify the output current from the photodiode. The APD produces a relatively larger current by introducing significant photon amplification. Through preliminary analysis, it is believed that PIN + TIA is more commonly used in short-to-medium reach transmission systems, because its amplification noise is generally smaller than that of APD. However, when the received optical power is very low, APD with high detection sensitivity may be more suitable to detect the signal than PIN + TIA. At present, most of the reported 100-Gbit/s even 200-Gbit/s short-reach transmission systems had applied single-end PD as the receiver component.

3.2. Single-End Photodetector under Kramers-Kronig Direct Detection

As mentioned above, single-end PD in conventional IM/DD transmission systems is only used to detect signal intensity. Therefore, even various complex equalization techniques are used to assist signal demodulation; the single-end PD based transmission systems are still limited to tens of kilometers, since the CD effect would lead to serious inter-symbol interference. An effective way to compensate the dispersion is to insert an optical dispersion compensation module in the transmission link, but extra insertion loss and component cost will be introduced for cost-sensitive short-reach transmission systems. Currently, an alternative approach, Kramers-Kronig direct detection [18,92–100], has been investigated, as it can reconstruct the intensity and phase of the received signal

from the intensity measurement. Figure 5 shows the Kramers-Kronig direct detection scheme. The received signal, which consists of an optical carrier *c* and a modulated signal under bandwidth *B*, is directly detected by a single-end PD. The output analog signal is proportional to the optical intensity. After the conversion from analog signal to digital signal by ADC, the complex digital signal can be reconstructed by digital signal processing (DSP). Once the phase and amplitude information are reconstructed, the conventional DSP algorithms (e.g., CD compensation, fiber nonlinearity compensation, polarization demultiplexing, carrier phase recovery, et al.) based on coherent receiver can be applied to mitigate channel distortions. Therefore, the use of the Kramers-Kronig direct detection in transmission system would be able to extend the transmission distance and transmission rate. At present, many research groups around the world have implemented Kramers-Kronig direct detection in short-reach transmission systems, even in metro and long-haul transmission systems. Z. Li et al. achieved four-channel 168-Gbit/s 64-QAM Nyquist-SCM transmission using a 40-GHz single-end PIN photodiode [96]. X. Chen et al. demonstrated 125-km SMF transmission in a four-channel 240-Gbit/s polarization division multiplexing (PDM) 32-QAM system by using a 24-GHz photodiode [97]. K. Schuh et al. transmitted a line rate of 450-Gbit/s 32-QAM signal detected by a ~85-GHz bandwidth photodiode over 480-km SMF [98]. Assisted by a sparse I/Q Volterra filter algorithm, L. Shu et al. experimentally demonstrated 112-Gbit/s 16-QAM transmission over 960-km SSMF based on a 50-GHz bandwidth photodiode [99]. Additionally, S. Le et al. demonstrated 1.6-Tbit/s 8-channel 16-QAM transmission with 1200-km Corning®TXF™ fiber link by using a 3-dB bandwidth of ~80-GHz photodiode [100]. The bandwidth of the receiver component needs to be at least twice the signal bandwidth, while that of ADC also needs to meet the demands. Although the Kramers-Kronig direct detection scheme with simple receiver structure and high sensitivity is argued to be a potential solution for high-speed short-reach transmission systems, the receiver cost may be an important factor hindering its practical application.

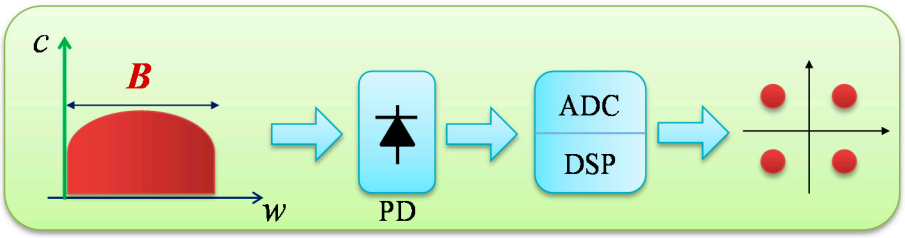

Figure 5. Kramers-Kronig direct detection scheme; PD: photodetector; ADC: analog to digital converter; DSP: digital signal processing module.

3.3. Stokes Vector Direct Detection

Another advanced direct detection scheme, Stokes vector direct detection, has recently gained much attraction in beyond 100-Gbit/s short-reach and metro transmission systems. It has been proposed to realize linear complex optical channels as well as enhance transmission reach and system capacity. As depicted in Figure 6a, the structure I of Stokes vector direct detection applied one polarization beam splitter (PBS), one optical 90° hybrid and three balance photodetectors (BPDs) to obtain three important Stokes vectors (e.g., S_1, S_2, S_3). In fact, Stokes vector direct detection can be generalized by any three or four detections of polarization states as long as they were nonsingular superpositions of Stokes vector components. Here, Figure 6b showed a structure that consisted of one optical 90° hybrid and four single-ended PDs. The structure can provide four outputs obtaining $|X|^2$, $|Y|^2$, $|X + Y|^2$, and $|X + iY|^2$, and then these components can be linearly converted to the three components S_1, S_2, and S_3 of Stokes vector. Another structure using four single-ended PDs and three polarizers is shown in Figure 6c, where the signal intensity of different polarization states are detected, and then the four outputs can be linearly converted to Stokes vector. The applications of these structures have been proposed and verified in various high-speed transmission systems. For example, M. Morsy-Osman et al. proposed

a three BPDs-based structure (structure I) for Stokes vector direct detection for the first time, and experimentally verified in a 224-Gbit/s PDM-PAM-4 transmission system over 10-km SMF assisted by a single 1310-nm laser and a silicon photonic intensity modulator [19]. Furthermore, this group proposed a novel reduced-complexity single-stage SSBI cancellation algorithm to enhance the transmission rate to 480-Gbit/s and transmission distance to 80-km SMF [101]. On the other hand, D. Che et al. further proposed another Stokes vector direct detection solution (structure II) based on four PDs and one optical hybrid [20], which was then verified in a 1T-Gbit/s PS-64QAM 100-km transmission system assisted by three-dimensional signal field recovery [102]. Furthermore, K. Kikuchi et al. proposed a novel Stokes vector receiver configuration (structure III) with four PDs and three polarizers. Based on the configuration, the polarization tracking and demultiplexing operations had been successfully verified in polarization multiplexing IM/DD transmission systems [21]. Moreover, based on the receiver configuration, Y. Pan et al. proposed an efficient and low-cost simplified detection solution, which was demonstrated in 160-Gbit/s 2 × PDM-PAM-4 transmission system over 25-km NZDSF [103]. Generally, the Stokes vector direct detection, which can realize two-dimensional even three-dimensional detection, provides a compromise between one-dimensional direct detection and four-dimensional coherent detection.

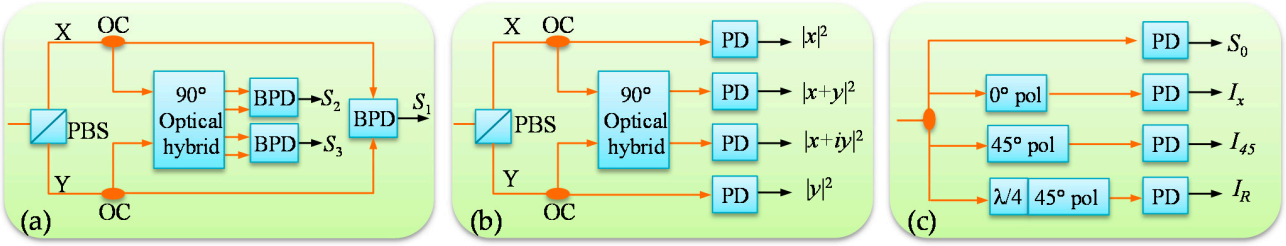

Figure 6. Different structures of Stokes vector direct detection: (**a**) structure I [19]; (**b**) structure II; (**c**) structure III [21]; PBS: polarization beam splitter; OC: optical coupler; BPD: balanced photodetector; pol: polarizer.

3.4. Monolithic Integrated Receiver

Various detection methods with discrete components have been applied and demonstrated in short-reach transmission systems. In order to further reduce footprint size, costm and power consumption, many efforts are being made to push discrete components to monolithic integration in both InP-based and SiP-based monolithic integration [104]. Recently, based on a silicon-on-insulator platform, Y. Ding et al. demonstrated a waveguide-coupled integrated graphene plasmonic photodetector with beyond 110-GHz bandwidth [22]. C. Ferrari et al. demonstrated a 400-Gbit/s (16-channels 25-Gbit/s OOK) receiver where PIN + TIA arrays were integrated on a silicon PLC platform [105]. For another alternative cost-effective receiver, S. Ghosh et al. proposed and demonstrated an InGaAsP/InP waveguide-based polarization-analyzing circuit in integrated Stokes vector receiver [106]. Figure 7a depicted a schematic top-view of the proposed InP-based Stokes vector receiver, where a 1 × 4 multimode interference (MMI) splitter was used to split the input light equally into four ports. As illustrated in Figure 7b,c, through the Stokes vector converter (SVC) sections consisting of a symmetric waveguide (SW) and a half-ridge asymmetric waveguide (ASW), the light can be converted into four different states depending on the design of SVC. Finally, these four output lights were detected by four polarization-selective PDs (PS-PDs), which had higher sensitivity for the transverse-electric (TE) mode than the transverse-magnetic (TM) mode. Four basis vectors were located at the vertices of a regular tetrahedron inscribed on the Poincaré sphere as depicted in Figure 7d. The application of the integrated Stokes vector receiver had been demonstrated in 10-Gbaud transmission systems. In addition, F. Zhang et al. reported the first PDM Kramers-Kronig coherent receiver in photonic integrated circuit with a capability to detect 256-Gbit/s 16-QAM signal, which showed the most compact size among silicon coherent

receivers [107]. We find that monolithic integrated receiver not only makes monolithic integrated detection chips practically feasible, but also makes it excel discrete components in many aspects, including cost, power consumption, and footprint.

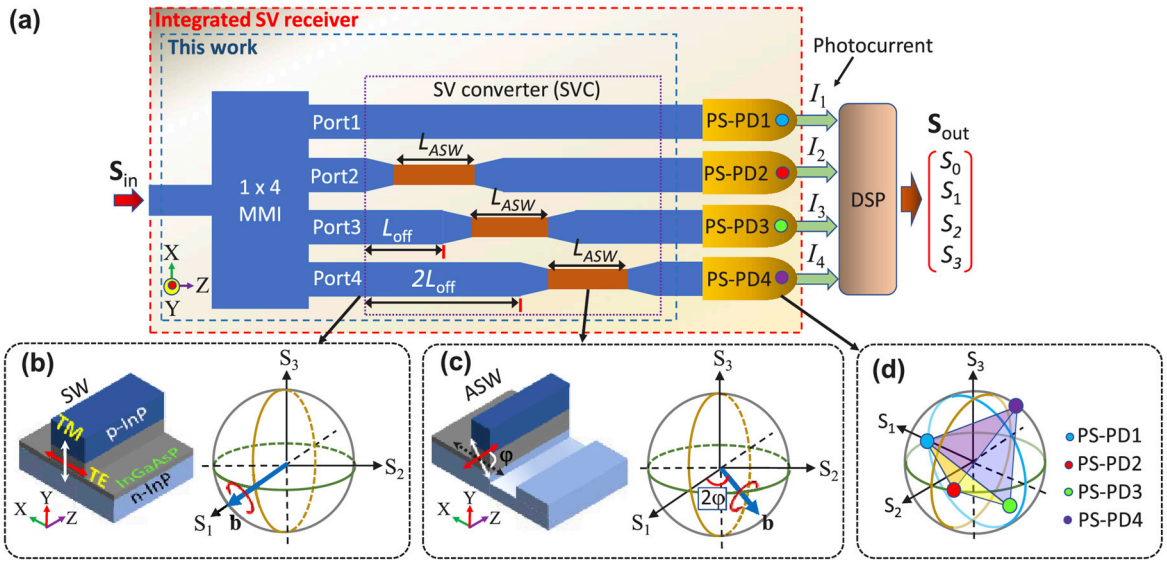

Figure 7. (**a**) Schematic top-view (XZ-plane) of the integrated Stokes vector receiver on InP; (**b**) symmetric waveguide (SW) and (**c**) asymmetric waveguide (ASW) used in the receiver; (**d**) illustrations of four basis vectors on the Poincaré sphere; MMI: multimode interference; SV: Stokes vector; PS-PD: polarization-selective PD; TE: transverse-electric; TM: transverse-magnetic; (From [106] © 2021 OSA).

4. Some Integrated Solutions for Short-Reach Transmission Systems

4.1. Simplified Detection Scheme

A simplified detection scheme consisting of a Stokes vector receiver, an optical band-pass filter, and a single-end PD had been proposed to simultaneously detect two channels PDM-PAM4 transmission signals [103]. The simplified scheme can reduce the number of receivers by half without sacrificing transmission capacity compared to Ref. [21], and the spectral efficiency can be doubled compared to Ref. [108]. The principle of the simplified detection scheme was shown in Figure 8. In the transmitter side, four independent PAM-4 signals with two optical carriers were combined to generate the 2 × PDM-PAM4 signals, whose state of polarizations (SOPs) consisted of 0°, 90°, −45°, and 45°. Here, the vector E_1, E_2, E_3, and E_4 represented the signal of 0°, 90°, 45°, and −45° SOP respectively. It is notable that there was a 90° phase difference between two orthogonal PDM signals to mitigate beating crosstalk at the receiver. After fiber transmission, the intensity signals that were received by Stokes vector receiver were I_{o1}, I_{o2}, I_{o3}, and I_{o4}. Two channels of transmission signals cannot be demultiplexed by a Stokes vector receiver. Here, an optical band pass filter (OBPF) and additional single-end PD were introduced to obtain intensity information I_5 of laser 1. Two channels of PDM-PAM4 transmission signals can be achieved for demultiplexing through these Stokes parameters and additional information.

The transmission performance of the 2 × PDM-PAM4 and the single PDM-PAM4 systems were measured as depicted in Figure 9. Here, the 2 × PDM-PAM4 signals transmitted over 25-km NZDSF link, and the transmission rate was set to 4 × 20-Gbit/s and 4 × 40-Gbit/s, respectively. Figure 9a showed the performance of 4 × 20-Gbit/s signals over 25-km NZDSF link. About 0.8-dB power penalty was observed between the 2 × PDM-PAM4 system and the single PDM-PAM4 system. As depicted in Figure 9b, about 1-dB power penalty can be obtained when transmission rate was up to 4 × 40-Gbit/s. We found that the performance degradation was limited as the bitrate increased from 4 × 20-Gbit/s to 4 × 40-Gbit/s over 25-km. In addition, the linear relationship between BER and received power is destroyed after

transmission. It may be that the received power was close to or beyond the saturation power of single-end PD. On the other hand, the performance difference between two orthogonal PDM-PAM4 signals became more apparent for 4 × 40-Gbit/s signals. The most likely reason was the influence of CD in spite of NZDSF used. Experimental demonstration had verified the effectiveness of the simplified detection scheme after 25-km fiber transmission and in the presence of polarization scrambling. We believe that such a scheme might be applied in short-reach transmission systems such as data center, access or metro network.

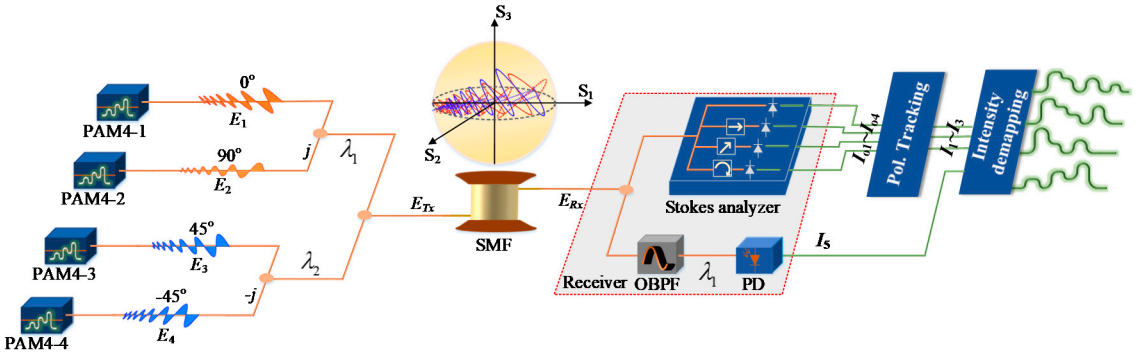

Figure 8. The principle of the simplified detection scheme. PAM: pulse amplitude modulation; SMF: single mode fiber; Pol.: polarization; OBPF: optical band-pass filter; PD, photodetector; (From [103] © 2021 OSA).

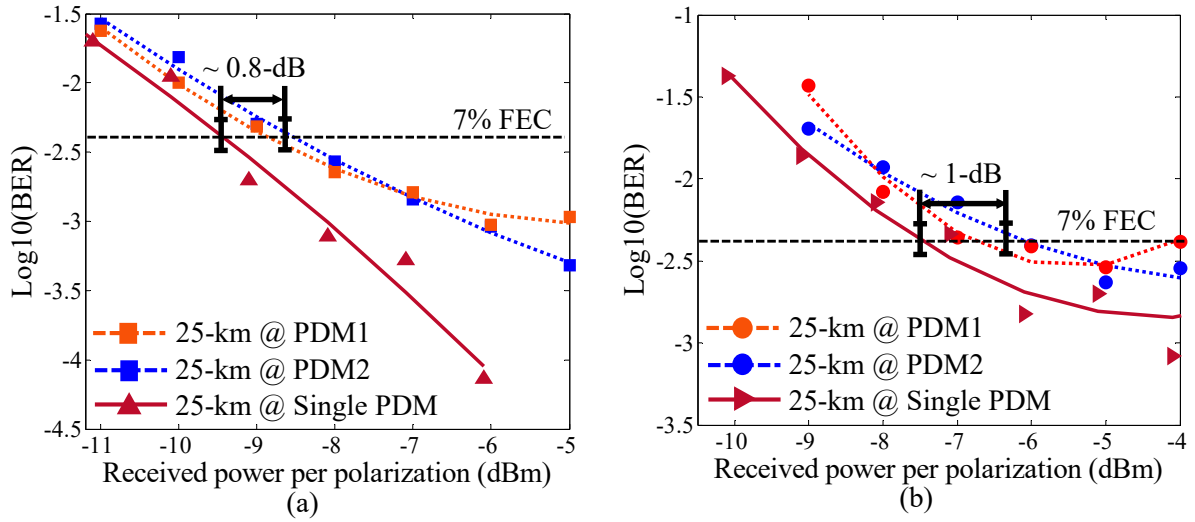

Figure 9. Twenty-five km transmission performance of the 2 × PDM-PAM4 and the single PDM-PAM4 systems. (**a**) BER at 4 × 20-Gbit/s and (**b**) 4 × 40-Gbit/s. PDM: polarization division multiplexing; FEC: forward error correction; (From [101] © 2021 OSA).

4.2. Transceiver Integration Scheme Based on Direct Detection

For IM/DD systems, the easiest way to increase transmission rate is to transmit multi-channel data streams in parallel, but this kind of system needs to use multiple sets of tranmitter and receiver components, which would lead to the increase of system cost to a certain extent. For reducing cost constraints, a transceiver integration solution based on direct detection, which can generate, transmit and detect multi-channel intensity signals at the same time, had been designed as depicted in Figure 10. The transmitter part of the transceiver integration solution, which consisted of multiple lasers, multiple drivers, and multiple MZM modulators, can generate multi-channels optical signals. After fiber transmission, the receiver part including multiple single-end PDs and multiple TIAs, would be able to detect multi-channel transmission signals. Based on this principle, T. Aoki et al. successfully demonstrated a 16 channels 25-Gbit/s OOK optical transceiver on package

SiP [28]. The photographs of electronic integrated circuit (EIC) and photonic integrated circuit (PIC) of the high-density 16 channels optical transceiver where transmitter and receiver components were highly integrated in the chips were shown in Figure 11a,b. At the transmitter section of the transceiver, multiple wavelength lights emitting from 4 × 4 channels laser diodes (LDs) were modulated by 2 × 8 Mach–Zehnder interferometer (MZI) modulators under push-pull type, which were driven by 2 × 8 electronic drivers, to generate 16 channels 25-Gbit/s OOK optical signals. Then, the multi-channel optical signals were fed into an array of 16 grating couplers by waveguides and coupled into 16 optical fiber transmission links, respectively. At the receiver side, multi-channel optical signals were coupled into the PIC waveguide through 16 grating couplers. Finally, the transmission signals were detected by 16 PDs and amplified by TIAs.

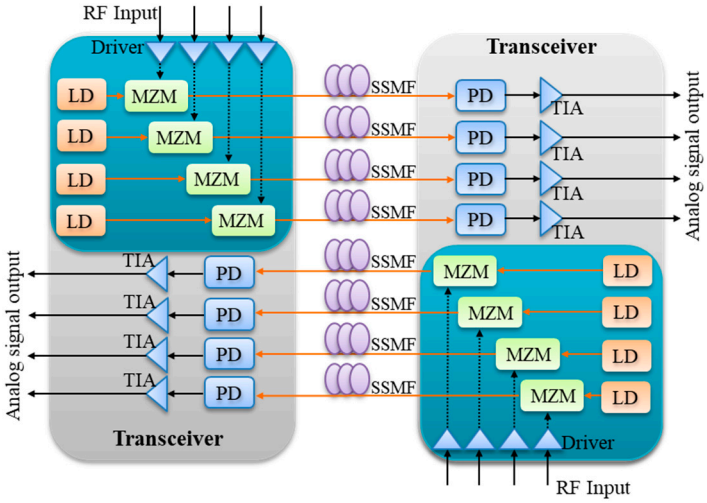

Figure 10. Block diagram of transceiver integration scheme based on direct detection. LD: laser diode; MZM: Mach-Zehnder modulator; RF: radio-frequency; SSMF: standard single mode fiber; TIA: trans-impedance amplifier; PD: photodetector.

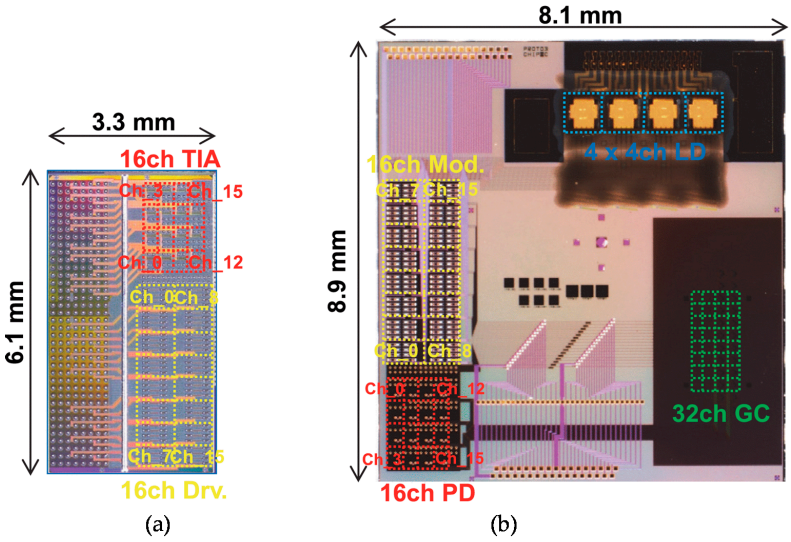

Figure 11. Photographs of (**a**) electronic integrated circuit (EIC) and (**b**) photonic integrated circuit (PIC) of the high-density 16 channels optical transceivers where transmitter and receiver elements were highly integrated in the chips; 4 × 4 channels laser diodes (LDs) were assembled and 32 channels (32ch) grating couplers (GCs) were formed in the PIC; Ch_1: the first channel; Ch_2: the second channel; TIA: trans-impedance amplifier; (From [28] © 2021 IEEE).

In here, the performance of multi-channel transceivers was further evaluated by the eye diagram and BER. Figure 12a shows the optical eye diagrams of all transmitter channels, which depicted clear eye openings. Subsequently, the inter-channel crosstalk penalty among multi-channel transmitters was measured by a commercially available receiver module. The channel 4 (ch_4) were selected as a victim channel to study the effect of a crosstalk penalty from other aggressor transmitter channels. As shown in Figure 12b, the sensitivity changes of ch_4 were measured at multi-channel transmitters operations. The total penalty between all channels driving and only ch_4 driving was about 1.4-dB, and it was considered to be negligible in high-density assembled configuration. Next, receiver performance of the transceiver was verified though a discrete transmitter including a $LiNbO_3$ MZM modulator and a laser. The optical eye diagrams were detected by all receiver channels of the transceiver as depicted in Figure 13a. Just like the transmitter side, when all receiver channels were operated, the sensitivity of the test channel can be found to be slightly degraded, and the 1.4-dB penalty can be observed in Figure 13b.

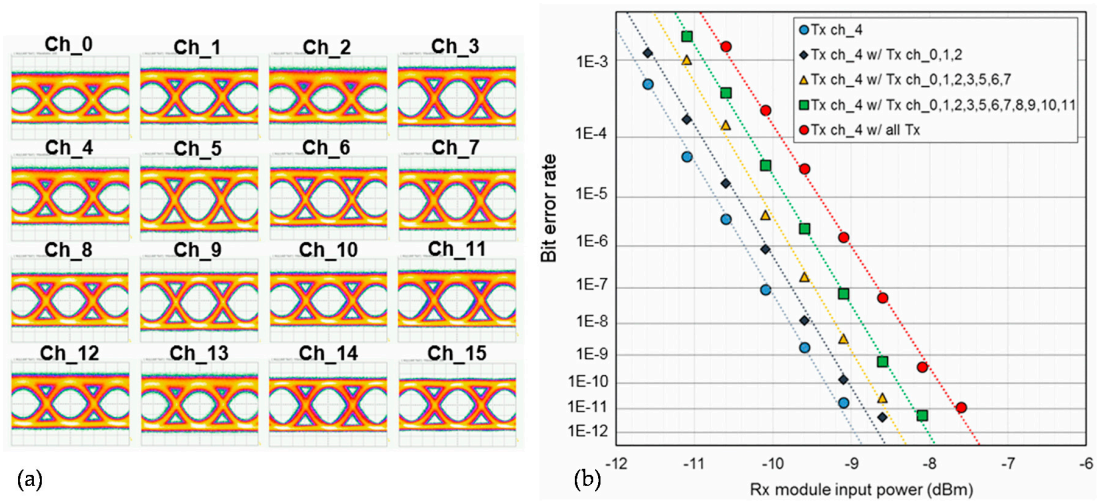

Figure 12. (**a**) Optical eye diagrams of all transmitter channels and (**b**) the sensitivity changes of ch_4 at multi-channel transmitters operations; Ch_1: the first channel; TX: transmitter; Rx: receiver; (From [28] © 2021 IEEE).

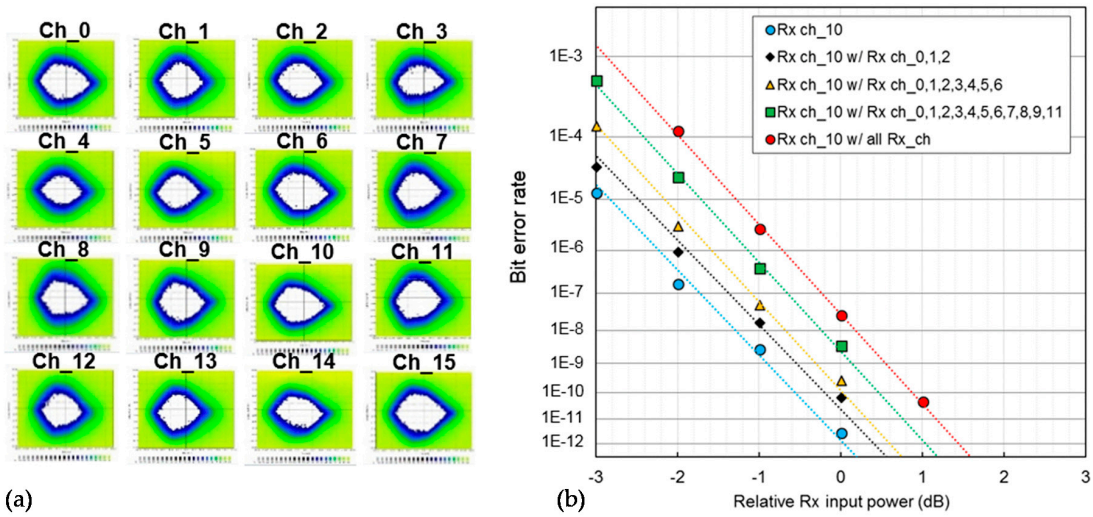

Figure 13. (**a**) Optical eye diagrams of all receiver channels and (**b**) BER performance under the first channel; TX: transmitter; Rx: receiver; (From [28] © 2021 IEEE).

4.3. Transceiver Integration Scheme Based on Coherent Detection

There is another alternative transceiver integration solution based on coherent detection [27], which had been designed as depicted in Figure 14. The PIC integrated two full coherent transmitter channels including two tunable lasers, four SOA amplifiers, two PDM-IQ modulators, four Mach-Zehnder modulator drivers, two full coherent receiver channels containing two tunable lasers, two 90° hybirds, eight BPDs, and four TIAs in a single InP-based chip. It is noticed that the transmitter and receiver on the PIC integrated two lasers respectively. The main purpose was to be able to tune the wavelength and output power of the laser on the transmitter and receiver independently, as such it was more suitable for a reconfigurable optical network rather than a shared laser solution between transmitter and receiver. In addition, the two channel transceivers integration scheme had been further demonstrated in a two channels 800-Gbit/s multi-subcarrier transmission system [27]. As shown in Figure 15a, the transmitter part driven by a 100-GSa/s digital to analog converter (DAC) generated a 800-Gbit/s/ wavelength 8 subcarriers (SC), and each subcarrier supported 100-Gbit/s probabilistic shaping (PS) -64-QAM signal so that a total capacity of 800-Gbit/s per wavelength can be obtained. The optical spectra of transmitter in Figure 15b showed a single ~95-GHz wide channel with eight digital subcarriers, where SC1 represented the first subcarrier. Following the optical amplifier, the output optical signal was coupled into the receiver part of the transceiver to realize coherent detection operation, and the detected signal after TIA was connected to a set of real-time scopes operating at 200-GSa/s. Then, the channel impairments were equalized and compensated by offline DSP module. Overall Q_2 factor of the received signal was measured to be about 7.5-dB under back-to-back conditions, which indirectly proved that there was enough margin for fiber transmission. All subcarrier PS-64QAM constellations after impairments compensation were inserted in Figure 15c.

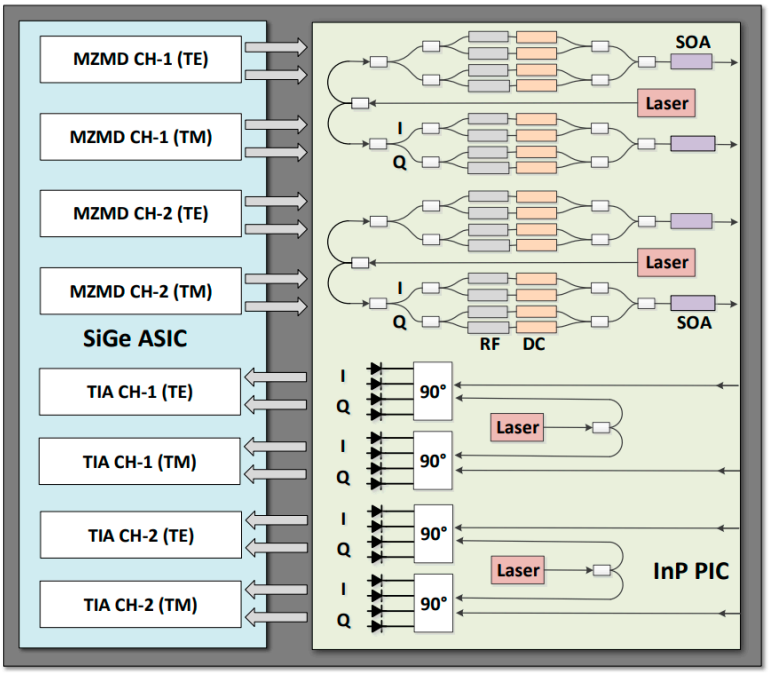

Figure 14. Schematic of transceiver integration scheme based on coherent detection; MZMD: Mach Zehnder modulator driver; TE: transverse-electric; TM: transverse-magnetic; TIA: trans-impedance amplifier; RF: radio-frequency; DC: direct current; InP: Indium phosphide; PIC: photonic integrated circuit; SOA: semiconductor optical amplifier; Ch_1: the first channel; (From [27] © 2021 IEEE).

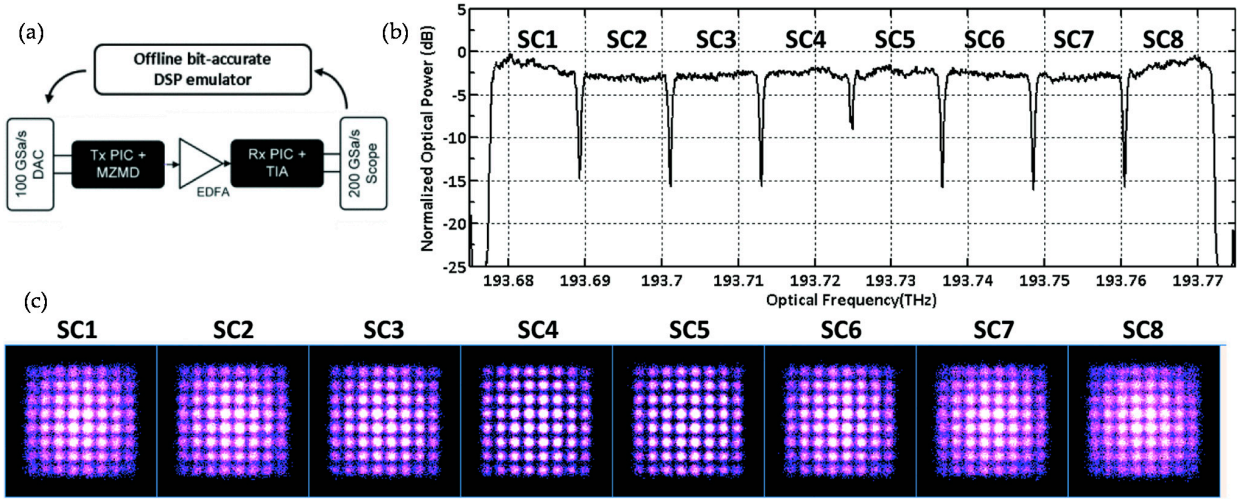

Figure 15. (**a**) Experimental setup for 800-Gbit/s transmission measurements; (**b**) optical spectra showing a single ~95-GHz wide channel with eight digital subcarriers (from SC1 to SC8); (**c**) all received eight subcarrier probabilistic shaping 64-QAM constellations; DAC: digital to analog converter; Table 1. the first subcarrier; DSP: digital signal processing; MZMD: Mach Zehnder modulator driver; PIC: photonic integrated circuit; TIA: trans-impedance amplifier; (From [27] © 2021 IEEE).

5. Discussion

It is well-known that short-reach transmission systems are extremely sensitive to cost of components due to the enormous scale of deployments in intra- and inter-data center optical interconnects. Thus, optical transmitters and receivers at low-cost are required in these applications. To select cost-effective transmitter and receiver components more equitably, the technology and component options based on different transmission distances have been summarized in Figure 16. Note that the cost of components usually includes material cost, yield rate, packaging cost, test cost, design cost, and so on. Most of these costs are difficult to predict in the actual production process, thus it is hard to calculate the accurate cost of components. In this paper, the relative costs of various components are discussed.

With the development of low-cost coherent detection and monolithic integration technologies, VCSEL, DML, EML, MZM, IQ modulator, and monolithic integrated transmitter have been the major options to construct the transmitter of high-speed short-reach transmission systems. Here, we compare the supported wavelength λ, supported fiber type, transmission distance, bandwidth, frequency chirp, footprint, and relative cost of different transmitter components as depicted in Table 6. The transmission signal in C-band would be greatly affected by CD effect. In IM/DD transmission systems, since the transmission signal is often a double sideband, the interaction between square law detection in single-end PD and CD would produce fiber power fading, which may cause severe ISI contributions to their adjacent symbols. In addition, since the electrical signals of direct modulation components such as VCSEL and DML are directly applied to their laser cavities, these components whose responses were caused by transient chirp and adiabatic chirp would show a higher frequency chirp than EML caused by transient chirp. While, for external modulation components such as MZM, IQ modulator and monolithic integrated transmitter, the frequency chirp does not exist. The interplay between the frequency chirp and CD would induce severe nonlinear distortions and lead to serious degradation of transmission performance. To deal with these problems, DML is applied in mostly <40-km O-band high-speed transmission systems as summarized in Tables 2 and 6. In addition, the application of VCSEL is mostly used in hundreds of meters of 850-nm few-/multi-mode transmission systems so that the influence of CD can be weakened to a certain extent. It is generally believed that the combination of MM-VCSEL and MMF has been recognized as a highly effective solution for <300-m short-reach optical interconnects.

Certainly, the SM-VCSEL combining MMF or SMF system can support a few kilometers transmission distance. On the other hand, the bandwidth is another important factor in the selection of transmitter components. As depicted in Table 5, the bandwidth of monolithic integrated transmitter is usually greater than 40-GHz. Generally, despite many efforts made to achieve beyond 100-Gbit/s per lane signal transmission, the common bandwidth of VCSEL is around 25-GHz, as shown in Table 1, while that of DML is less than 30-GHz in Table 2. To break the DML bandwidth ceiling of around 30 GHz, special physical effects including detuned-loading and photon-photon resonance have been introduced to enhance the laser response in the high frequency region, and the state-of-art bandwidth of DML can be up to 100-GHz [47]. As depicted in Tables 3 and 4, the common bandwidths of MZM and EML are beyond 30-GHz in beyond 100-Gbit/s per lane transmission systems, although the state-of-art bandwidth 100-GHz of EML had been reported [13]. In general, for hundreds of meters of high-speed intra-data center optical interconnects, VCSEL with low-cost and small footprint size is commonly considered as the best candidate transmitter. For a few and tens of kilometers high-speed optical interconnects, the best choice becomes unobvious between DML and EML. Of course, in terms of cost, a few kilometers high-speed optical interconnects prefer to use DML. In here, for the cost-sensitive short-reach transmission systems, $LiNbO_3$-based MZM and IQ modulator with large footprint size and high-cost may not be the best transmitter option. Currently, with the help of monolithic integration technology, the MZM and IQ modulator-based monolithic integrated transmitters based on InP-based monolithic integration or SiP have shown irreplaceable advantages in cost, package, bandwidth, and transmission distance compared with other transmitters. Therefore, we believe that the monolithic integrated transmitters have the potential to gradually replace other transmitters in high-speed short-reach transmission systems in the future, especially in tens of kilometers of high-speed optical interconnects.

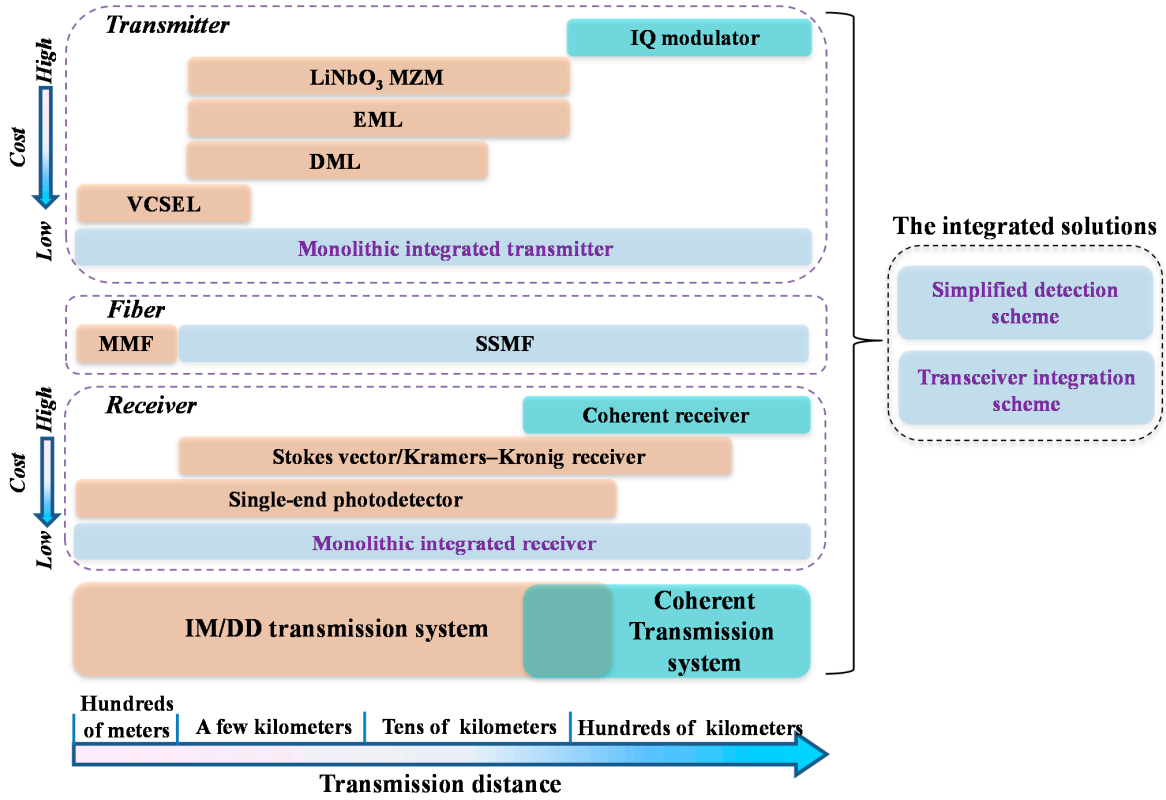

Figure 16. The technological and component options for high-speed short-reach transmission systems.

Table 6. Comparison of different transmitters applied in beyond 100-Gbit/s per lane data transmission.

Tx	λ	Fiber	Reach	BW	Chirp	Footprint	Cost
IQ Modulator	O-/C-Band	SMF	>80 km	high	–	high	high
MZM	O-/C-Band	SMF	<80 km	high	–	high	high
EML	O-/C-Band	SMF	<80 km	high	low	moderate	moderate
DML	Mostly O-Band Partially C-Band	SMF	<40 km	moderate	high	low	low
VCSEL	Mostly 850 nm Partially C-Band	MMF/SMF	<300 m <2 km	low	high	low	Very low
Monolithic integrated transmitter	O-/C-Band	SMF	whole range	high	–	low	moderate

In recent years, various receivers such as single-end PD, Kramers-Kronig receiver, Stokes vector receiver, coherent receiver, and monolithic integrated receiver have been widely reported in beyond 100-Gbit/s short-reach transmission systems. Here, as depicted in Table 7, we compare the supported transmission distance, detection sensitivity, footprint, and cost of different receiver components in beyond 100-Gbit/s per lane transmission system. For the IM/DD transmission system, beyond 100-Gbit/s researches mainly use the single-end PD with low-cost to detect the transmission signals. The single-end PD can only detect intensity information, and its applications are often limited to less than tens of kilometers of transmission distance because CD effect would lead to serious inter-symbol interference. While, this phenomenon may be even worse for high-speed transmission links as these links can be more sensitive to signal impairments. Many advanced direct detection technologies such as Kramers-Kronig receiver and Stokes vector receiver have been proposed and studied extensively, and the gap between conventional direct detection and advanced coherent detection is getting closer. Since these techniques can reconstruct the complex domain of the modulation signal, the CD effect can be compensated in the DSP module of receiver side. Meanwhile, to combine complex vector modulation with polarization division multiplexing, the rate-distance product can be further improved. Despite these advanced direct detection technologies having large footprint size and moderate cost compared to a single-end PD, they still show the potential in certain application scenarios. Coherent receiver with high detection sensitivity has the ability to achieve high rate-distance product, but its cost is too high to use directly in cost-sensitive short-reach transmission systems. In recent years, InP/SiP-based monolithic integrated receivers incorporating various schemes, such as single-end PD, Kramers-Kronig receiver, Stokes vector receiver, and coherent receiver have been widely reported and have the advantages of low-cost and small footprint size. Furthermore, some effective solutions combining simplified direct scheme and transceiver integration scheme have also been reported in short-reach transmission systems for the purpose of cost and energy effectiveness.

Table 7. Comparison of different receiver components applied in beyond 100-Gbit/s per lane data transmission.

Rx	Reach	Footprint	Sensitivity	Cost
Coherent receiver	high	high	high	high
Stokes vector receiver	moderate	moderate	moderate	moderate
Kramers-Kronig receiver	moderate	moderate	moderate	moderate
Single-end PD	low	low	low	low
Monolithic integrated receiver	whole range	low	whole range	Very low

6. Conclusions

In this paper, we review the mainstream transmitter components (e.g., VCSEL/DML/EML/MZM/monolithic integrated transmitter) and receiver components (e.g., single-end photodetector/Kramers-Kronig receiver/Stokes vector receiver/monolithic integrated receiver). Next, a simplified detection scheme and two transceiver integration schemes under direct and coherent detection have been presented in detail. Then, we further summarize and discuss the technological and component options based on different transmission distances. We found that monolithic integrated components, especially transceiver integration, can dramatically reduce component cost. Therefore, we believe that such components would

show great potential in the next-generation short-reach transmission systems. In addition, with the cost of coherent detection technology sinking, we predict that transceiver integration scheme based on coherent detection will become the mainstream scheme of beyond 400-Gbit/s short-reach data transmission in the future.

Author Contributions: L.J. and L.Y. contributed to the idea. L.J., L.Y., Y.P., and A.Y., contributed to the writing of the manuscript. B.Z., Q.H., W.P., and B.L. contributed to the reviewing and editing of the manuscript. L.Y. supervised the project. All authors have read and agreed to the published version of the manuscript.

Funding: This research is supported by the National Key Research and Development Program of China (2019YFB1803500), and National Natural Science Foundation of China (NSFC) (61860206006, 62005228).

Data Availability Statement: Data sharing not applicable.

Conflicts of Interest: The authors declare no conflict of interest.

References

1. Al-Turjman, F.; Ever, E.; Zahmatkesh, H. Small Cells in the Forthcoming 5G/IoT: Traffic Modelling and Deployment Overview. *IEEE Commun. Surv. Tutor.* **2019**, *21*, 28–65. [CrossRef]
2. Kachris, C.; Kanonakis, K.; Tomkos, I. Optical interconnection networks in data centers: Recent trends and future challenges. *IEEE Commun. Mag.* **2013**, *51*, 39–45. [CrossRef]
3. Briscoe, B.; Brunstrom, A.; Petlund, A.; Hayes, D.; Ros, D.; Tsang, J.; Gjessing, S.; Fairhurst, G.; Welzl, M. Reducing internet latency: A survey of techniques and their merits. *IEEE Commun. Surv. Tutor.* **2014**, *18*, 2149–2196. [CrossRef]
4. Eiselt, M.H.; Eiselt, N.; Dochhan, A. Direct Detection Solutions for 100G and Beyond. In Proceedings of the Optical Fiber Communication Conference, Los Angeles, CA, USA, 19–23 March 2017; p. Tu3I.3.
5. Ledentsov, N.N.; Shchukin, V.A.; Kalosha, V.P.; Ledentsov, N., Jr.; Chorchos, L.; Turkiewicz, J.P.; Hecht, U.; Kurth, P.; Gerfers, F.; Lavrencik, J.; et al. Optical Interconnects Using Single-Mode and Multi-Mode VCSEL and Multi-Mode Fiber. In Proceedings of the Optical Fiber Communication Conference, San Diego, CA, USA, 8–12 March 2020; p. M3D.1.
6. Zuo, T.; Zhang, L.; Zhou, J.; Zhang, Q.; Zhou, E.; Liu, G.N. Single Lane 150-Gb/s, 100-Gb/s and 70-Gb/s 4-PAM Transmission over 100-m, 300-m and 500-m MMF Using 25-G Class 850nm VCSEL. In Proceedings of the European Conference on Optical Communication, Dusseldorf, Germany, 18–22 September 2016; pp. 1–3.
7. Tatum, J.A.; Landry, G.D.; Gazula, D.; Wade, J.K.; Westbergh, P. VCSEL-Based Optical Transceivers for Future Data Center Applications. In Proceedings of the Optical Fiber Communication Conference and Exhibition, San Diego, CA, USA, 11–15 March 2018; p. M3F.6.
8. Wang, W.; Zhao, P.; Zhang, Z.; Li, H.; Zang, D.; Zhu, N.; Lu, Y. First Demonstration of 112 Gb/s PAM-4 Amplifier-free Transmission over a Record Reach of 40 km Using 1.3 μm Directly Modulated Laser. In Proceedings of the Optical Fiber Communication Conference Postdeadline Papers, San Diego, CA, USA, 11–15 March 2018; p. Th4B.8.
9. Xu, Z.; Sun, C.; Ji, T.; Ji, H.; Shieh, W. Cascade Recurrent Neural Network Enabled 100-Gb/s PAM4 Short-Reach Optical Link Based on DML. In Proceedings of the Optical Fiber Communication Conference, San Diego, CA, USA, 8–12 March 2020; p. W2A.45.
10. Wei, Y.; Yu, J.; Shi, J.; Zhang, J.; He, J.; Chen, L. Demonstration of C-band 112G PAM-4 transmission over 80-km stand-single mode fiber based on direct-detection. *Opt. Commun.* **2018**, *424*, 32–36.
11. Estaran, J.; Rios-Mueller, R.; Mestre, M.A.; Jorge, F.; Mardoyan, H.; Konczykowska, A.; Dupuy, J.-Y.; Bigo, S. Artificial Neural Networks for Linear and Non-Linear Impairment Mitigation in High-Baudrate IM/DD Systems. In Proceedings of the European Conference on Optical Communication, Dusseldorf, Germany, 18–22 September 2016; pp. 1–3.
12. Nada, M.; Yoshimatsu, T.; Muramoto, Y.; Ohno, T.; Nakajima, F.; Matsuzaki, H. 106-Gbit/s PAM4 40-km Transmission Using an Avalanche Photodiode with 42-GHz Bandwidth. In Proceedings of the Optical Fiber Communication Conference, San Diego, CA, USA, 11–15 March 2018; p. W4D.2.
13. Chaciński, M.; Westergren, U.; Stoltz, B.; Thylén, L.; Schatz, R.; Hammerfeldt, S. Monolithically Integrated 100 GHz DFB-TWEAM. *IEEE J. Lightwave Technol.* **2009**, *27*, 3410–3415. [CrossRef]
14. Chan, T.K.; Way, W.I. 112 Gb/s PAM4 transmission over 40km SSMF using 1.3 μm gain-clamped semiconductor optical amplifier. In Proceedings of the Optical Fiber Communication Conference, Los Angeles, CA, USA, 22–26 March 2015; p. TH3A.4.
15. Lange, S.; Wolf, S.; Lutz, J.; Altenhain, L.; Schmid, R.; Kaiser, R.; Koos, C.; Randel, S.; Schell, M. 100 GBd Intensity Modulation and Direct Detection with an InP-based Monolithic DFB Laser Mach-Zehnder Modulator. In Proceedings of the Optical Fiber Communication Conference Postdeadline Papers, Los Angeles, CA, USA, 19–23 March 2017; p. Th5C.5.
16. Yamazaki, H.; Nagatani, M.; Wakita, H.; Ogiso, Y.; Nakamura, M.; Ida, M.; Nosaka, H.; Hashimoto, T.; Miyamoto, Y. IMDD transmission at net data rate of 333 Gb/s using over-100-GHz-bandwidth analog multiplexer and Mach–Zehnder modulator. *IEEE J. Lightwave Technol.* **2019**, *37*, 1772–1778. [CrossRef]

17. Li, Z.; Erkılınç, M.S.; Shi, K.; Sillekens, E.; Galdino, L.; Thomsen, B.C.; Bayvel, P.; Killey, R.I. SSBI Mitigation and the Kramers-Kronig Scheme in Single-Sideband Direct-Detection Transmission With Receiver-Based Electronic Dispersion Compensation. *IEEE J. Lightwave Technol.* **2017**, *35*, 1887–1893. [CrossRef]
18. Mecozzi, A.; Antonelli, C.; Shtaif, M. Kramers-Kronig coherent receiver. *Optica* **2016**, *3*, 1220–1227. [CrossRef]
19. Chagnon, M.; Osman, M.; Patel, D.; Veerasubramanian, V.; Samani, A.; Plant, D. 1λ 6 bits/symbol 280 and 350 Gb/s direct detection transceiver using intensity modulation polarization multiplexing and inter-polarization phase modulation. In Proceedings of the Optical Fiber Communication Conference Postdeadline Papers, Los Angeles, CA, USA, 22–26 March 2015; p. Th5B.2.
20. Che, D.; Li, A.; Chen, X.; Hu, Q.; Wang, Y.; Shieh, W. Stokes vector direct detection for linear complex optical channels. *IEEE J. Lightwave Technol.* **2015**, *33*, 678–684. [CrossRef]
21. Kikuchi, K. Electronic polarization-division demultiplexing based on digital signal processing in intensity-modulation direct-detection optical communication systems. *Opt. Express* **2014**, *22*, 1971–1980. [CrossRef]
22. Ding, Y.; Cheng, Z.; Zhu, X.; Yvind, K.; Dong, J.; Galili, M.; Hu, H.; Mortensen, N.A.; Xiao, S.; Oxenløwe, L.K. Ultra-compact integrated graphene plasmonic photodetector with bandwidth above 110 GHz. *Nanophotonics* **2019**. [CrossRef]
23. Ghosh, S.; Kawabata, Y.; Tanemura, T.; Nakano, Y. Polarization-analyzing circuit on InP for integrated Stokes vector receiver. *Opt. Express* **2017**, *25*, 12303–12310. [CrossRef] [PubMed]
24. Pang, X.; Ozolins, O.; Lin, R.; Zhang, L.; Udalcovs, A.; Xue, L.; Schatz, R.; Westergren, U.U.; Xiao, S.; Hu, W.; et al. 200 Gbps/Lane IM/DD Technologies for Short Reach Optical Interconnects. *IEEE J. Lightwave Technol.* **2020**, *38*, 492–503. [CrossRef]
25. Cheng, Q.; Bahadori, M.; Glick, M.; Rumley, S.; Bergman, K. Recent advances in optical technologies for data centers: A review. *Optica* **2018**, *5*, 1354–1370. [CrossRef]
26. Doerr, C.; Chen, L.; Vermeulen, D.; Nielsen, T.; Azemati, S.; Stulz, S.; McBrien, G.; Xu, X.; Mikkelsen, B.; Givehchi, M.; et al. Single-Chip Silicon Photonics 100-Gb/s Coherent Transceiver. In Proceedings of the Optical Fiber Communication Conference Postdeadline Papers, San Francisco, CA, USA, 9–13 March 2014; p. Th5C.1.
27. Lal, V.; Studenkov, P.; Frost, T.; Tsai, H.; Behnia, B.; Osenbach, J.; Wolf, S.; Going, R.; Porto, S.; Maher, R.; et al. 1.6Tbps Coherent 2-Channel Transceiver Using a Monolithic Tx/Rx InP PIC and Single SiGe ASIC. In Proceedings of the Optical Fiber Communication Conference, San Diego, CA, USA, 8–12 March 2020; p. M3A.2.
28. Aoki, T.; Sekiguchi, S.; Simoyama, T.; Tanaka, S.; Nishizawa, M.; Hatori, N.; Sobu, Y.; Sugama, A.T.; Akiyama, H.A.; Muranaka, H.; et al. Low-Crosstalk Simultaneous 16-Channel × 25 Gb/s Operation of High-Density Silicon Photonics Optical Transceiver. *IEEE J. Lightwave Technol.* **2018**, *36*, 1262–1267. [CrossRef]
29. Tatum, J.A.; Gazula, D.; Graham, L.A.; Guenter, J.K.; Johnson, R.H.; King, J.; Kocot, C.; Landry, G.D.; Lyubomirsky, I.; MacInnes, A.N.; et al. VCSEL-Based Interconnects for Current and Future Data Centers. *IEEE J. Lightwave Technol.* **2016**, *33*, 727–732. [CrossRef]
30. Haglund, E.; Westbergh, P.; Gustavsson, J.; Haglund, E.; Larsson, A. 30 GHz bandwidth 850 nm VCSEL with sub-100 fJ/bit energy dissipation at 25–50 Gbit/s. *Electron. Lett.* **2015**, *51*, 1096–1098. [CrossRef]
31. Puerta, R.; Agustin, M.; Chorchos, Ł.; Toński, J.; Kropp, J.-R.; Ledentsov, N.; Shchukin, N.V.A.; Ledentsov, N.N.; Henker, R.; Monroy, I.T.; et al. 107.5 Gb/s 850 nm multi- and single-mode VCSEL transmission over 10 and 100 m of multi-mode fiber. In Proceedings of the Optical Fiber Communication Conference Postdeadline Papers, Anaheim, CA, USA, 20–24 March 2016; p. Th5B.5.
32. Gebrewold, S.A.; Josten, A.; Baeuerle, B.; Stubenrauch, M.; Eitel, S.; Leuthold, J. PAM-8 108 Gbit/s Transmission Using an 850 nm Multi-Mode VCSEL. In Proceedings of the European Conference on Lasers and Electro-Optics, Munich, Germany, 25–29 June 2017; p. CI_4_6.
33. Dong, X.; Bamiedakis, N.; Cunningham, D.G.; Penty, R.V.; White, I.H. A Novel Equalizer for 112 Gb/s CAP-Based Data Transmission Over 150 m MMF Links. *IEEE J. Lightwave Technol.* **2019**, *37*, 5937–5944. [CrossRef]
34. Huang, W.; Chang, W.; Wei, C.; Liu, J.; Chen, Y.; Chi, K.; Wang, C.; Shi, J.; Chen, J. 93% Complexity Reduction of Volterra Nonlinear Equalizer by ℓ1-Regularization for 112-Gbps PAM-4 850-nm VCSEL Optical Interconnect. In Proceedings of the Optical Fiber Communications Conference and Exposition, San Diego, CA, USA, 11–15 March 2018; p. M2D.7.
35. Lavrencik, J.; Varughese, S.; Ledentsov, N.; Chorchos, Ł.; Ledentsov, N.N.; Ralph, S.E. 168Gbps PAM-4 Multimode Fiber Transmission through 50m using 28GHz 850nm Multimode VCSELs. In Proceedings of the Optical Fiber Communication Conference, San Diego, CA, USA, 8–12 March 2020; p. W1D.3.
36. Zuo, T.; Zhang, L.; Zhou, E.; Liu, G.N.; Xu, X. 112-Gb/s duobinary 4-PAM transmission over 200-m multi-mode fibre. In Proceedings of the European Conference on Optical Communication, Valencia, Spain, 27 September–1 October 2015; pp. 1–3. [CrossRef]
37. Zuo, T.; Zhang, T.; Zhang, S.; Liu, L. Single-lane 200-Gbps PAM-4 transmission for Datacenter Intra-Connections employing 850-nm VCSEL. In Proceedings of the Asia Communications and Photonics Conference, Beijing, China, 24–27 October 2020; p. S3H.2.
38. Ge, L.; Zhang, W.; Liang, C.; He, Z. Threshold-Based Pruned Retraining Volterra Equalization for 100 Gbps/Lane and 100-m Optical Interconnects Based on VCSEL and MMF. *IEEE J. Lightwave Technol.* **2019**, *37*, 3222–3228. [CrossRef]
39. Kottke, C.; Caspar, C.; Jungnickel, V.; Freund, R.; Agustin, M.; Ledentsov, N. High speed 160 Gb/s DMT VCSEL transmission using pre-equalization. In Proceedings of the Optical Fiber Communications Conference and Exhibition, Los Angeles, CA, USA, 19–23 March 2017; p. W4I.7.

40. Wu, B.; Zhou, X.; Ma, Y.; Jun, L.; Qiu, S.; Zhong, K.; Feng, Z.; Lu, C.; Vitaly, S. Single-Lane 112Gbps Transmission over 300m OM4 Multimode Fiber Based on A Single-Transverse-Mode 850nm VCSEL. In Proceedings of the European Conference on Optical Communication, Dusseldorf, Germany, 18–22 September 2016; pp. 1–3.
41. Pang, X.; Van Kerrebrouck, J.; Ozolins, O.; Lin, R.; Udalcovs, A.; Zhang, L.; Spiga, S.; Amann, M.; Van Steenberge, G.; Gan, L.; et al. 7×100 Gbps PAM-4 Transmission over 1-km and 10-km Single Mode 7-core Fiber using 1.5-μm SM-VCSEL. In Proceedings of the Optical Fiber Communications Conference and Exposition, San Diego, CA, USA, 11–15 March 2018; p. M1I.4.
42. Zhang, L.; Van Kerrebrouck, J.; Lin, R.; Pang, X.; Udalcovs, A.; Ozolins, O.; Spiga, S.; Amann, M.; Van Steenberge, G.; Gan, L.; et al. Nonlinearity Tolerant High-Speed DMT Transmission With 1.5-μm Single-Mode VCSEL and Multi-Core Fibers for Optical Interconnects. *IEEE J. Lightwave Technol.* **2019**, *37*, 380–388. [CrossRef]
43. Huang, C.; Wang, H.; Wu, C.; Cheng, C.; Tsai, C.; Wu, C. Comparison of High-Speed PAM4 and QAM-OFDM Data Transmission Using Single-Mode VCSEL in OM5 and OM4 MMF Links. *IEEE J. Sel. Top. Quantum Electron.* **2020**, *26*, 1500210. [CrossRef]
44. Simpanen, E.; Gustavsson, J.S.; Larsson, A.; Karlsson, M.; Sorin, W.V.; Mathai, S.; Bickham, S.R. 1060 nm single-mode VCSEL and single-mode fiber links for long-reach optical interconnects. *IEEE J. Lightwave Technol.* **2019**, *37*, 2963–2969. [CrossRef]
45. Li, M.; Li, K.; Chen, X.; Mishra, S.; Juarez, A.A.; Hurley, J.; Stone, J.; Wang, C.; Cheng, H.; Wu, C.; et al. Single-Mode VCSEL Transmission for Short Reach Communications. *IEEE J. Lightwave Technol.* **2020**. [CrossRef]
46. Matsui, Y.; Schatz, R.; Pham, T.; Ling, W.A.; Carey, G.; Daghighian, H.M.; Adams, D.; Sudo, T.; Roxlo, C. 55 GHz Bandwidth Distributed Reflector Laser. *IEEE J. Lightwave Technol.* **2017**, *35*, 397–403. [CrossRef]
47. Yamaoka, S.; Diamantopoulos, N.; Nishi, H.; Nakao, R.; Fujii, T.; Takeda, K.; Hiraki, T.; Kanazawa, S.; Tanobe, H.; Kakitsuka, T. 239.3-Gbit/s net rate PAM-4 transmission using directly modulated membrane lasers on high-thermal-conductivity Sic. In Proceedings of the European Conference on Optical Communication, Dublin, Ireland, 22–26 September 2019; pp. 1–4. [CrossRef]
48. Li, D.; Deng, L.; Ye, Y.; Zhang, Y.; Song, H.; Cheng, M.; Fu, S.; Tang, M.; Liu, D. Amplifier-free 4×96 Gb/s PAM8 transmission enabled by modified Volterra equalizer for short-reach applications using directly modulated lasers. *Opt. Express* **2019**, *27*, 17927–17939. [CrossRef]
49. Yan, W.; Li, L.; Liu, B.; Chen, H.; Tao, Z.; Tanaka, T.; Takahara, T.; Rasmussen, J.C.; Drenski, T. 80 km IM-DD transmission for 100 Gb/s per lane enabled by DMT and nonlinearity management. In Proceedings of the Optical Fiber Communication Conference, San Francisco, CA, USA, 9–13 March 2014; p. M2I.4.
50. Gao, Y.; Cartledge, J.C.; Yam, S.S.; Rezania, A.; Matsui, Y. 112 Gb/s PAM-4 Using a Directly Modulated Laser with Linear Pre-Compensation and Nonlinear Post-Compensation. In Proceedings of the European Conference on Optical Communication, Dusseldorf, Germany, 18–22 September 2016; p. M2.C2.
51. Diamantopoulos, N.; Diamantopoulos, N.; Yamazaki, H.; Yamaoka, S.; Nagatani, M.; Nishi, H.; Tanobe, H.; Nakao, R.; Fujii, T.; Takeda, K.; et al. Net 321.24-Gb/s IMDD Transmission Based on a >100-GHz Bandwidth Directly-Modulated Laser. In Proceedings of the Optical Fiber Communications Conference and Exhibition, San Diego, CA, USA, 8–12 March 2020; p. Th4C.1.
52. Che, D.; Matsui, Y.; Schatz, R.; Rodes, R.; Khan, F.; Kwakernaak, M.; Sudo, T.; Chandrasekhar, S.; Cho, J.; Chen, X.; et al. Direct Modulation of a 54-GHz Distributed Bragg Reflector Laser with 100-GBaud PAM-4 and 80-GBaud PAM-8. In Proceedings of the Optical Fiber Communications Conference and Exhibition, San Diego, CA, USA, 8–12 March 2020; p. Th3C.1.
53. Matsui, Y.; Schatz, R.; Che, D.; Khan, F.; Kwakernaak, M.; Tsurugi, S. Low-chirp isolator-free 65-GHz-bandwidth directly modulated lasers. *Nat. Photonics* **2021**, *15*, 59–63. [CrossRef]
54. Jiang, L.; Yan, L.; Yi, A.; Chen, Z.; Pan, Y.; Pan, W.; Luo, B.; Zhou, X.; Feng, X. Generation and transmission of PAM-PM signal using directly modulator laser for metro networks. In Proceedings of the Conference on Lasers and Electro-Optics, San Jose, CA, USA, 5–10 June 2016; p. SF2F.5.
55. Che, D.; Yuan, F.; Shieh, W. Towards High-order PAM Utilizing Large Frequency Chirp of Directly Modulated Lasers. In Proceedings of the Optical Fiber Communication Conference, Anaheim, CA, USA, 20–24 March 2016; p. W1A.4.
56. Gou, P.; Yu, J. A nonlinear ANN equalizer with mini-batch gradient descent in 40Gbaud PAM-8 IM/DD system. *Optical. Fiber Technol.* **2018**, *46*, 113–117. [CrossRef]
57. Zhang, L.; Zuo, T.; Mao, Y.; Zhang, Q.; Zhou, E.; Liu, G.N.; Xu, X. Beyond 100-Gb/s transmission over 80-km SMF using direct-detection SSB-DMT at C-band. *IEEE J. Lightwave Technol.* **2016**, *34*, 723–729. [CrossRef]
58. Mardoyan, H.; Mestre, M.A.; Estarán, J.; Jorge, F.; Blache, F.; Angelini, P.; Agnieszka, K.; Riet, M.; Virginie, N.; Jean-Yves, D.; et al. 84-, 100-, and 107-GBd PAM-4 Intensity-Modulation Direct-Detection Transceiver for Datacenter Interconnects. *IEEE J. Lightwave Technol.* **2017**, *35*, 1253–1259. [CrossRef]
59. Hu, Q.; Schuh, K.; Chagnon, M.; Buchali, F.; Bülow, H. 84 GBd Faster-Than-Nyquist PAM-4 transmission using only linear equalizer at receiver. In Proceedings of the Optical Fiber Communication Conference, San Diego, CA, USA, 3–7 March 2019; p. W4I.2.
60. Zhang, Q.; Stojanovic, N.; Xie, C.; Prodaniuc, C.; Laskowski, P. Transmission of single lane 128 Gbit/s PAM-4 signals over an 80 km SSMF link, enabled by DDMZM aided dispersion pre-compensation. *Opt. Express* **2016**, *24*, 24580–24591. [CrossRef] [PubMed]
61. Yamamoto, S.; Taniguchi, H.; Matsushita, A.; Nakamura, M.; Okamoto, S.; Kisaka, Y. Spectral-Shaping Technique Based on Nonlinear-Coded-Modulation for Short-Reach Optical Transmission. *IEEE J. Lightwave Technol.* **2020**, *38*, 466–474. [CrossRef]
62. Buchali, F.; Schuh, K.; Le, S.; Du, X.; Grözing, M.; Berroth, M. A SiGe HBT BiCMOS 1-to-4 ADC Frontend Supporting 100 GBaud PAM4 Reception at 14 GHz Digitizer Bandwidth. In Proceedings of the Optical Fiber Communications Conference and Exhibition, San Diego, CA, USA, 3–7 March 2019; p. Th4A.7.

63. Zhang, L.; Wei, J.; Stojanovic, N.; Prodaniuc, C.; Xie, C. Beyond 200-Gb/s DMT transmission over 2-km SMF based on a low-cost architecture with single-wavelength, single DAC/ADC and single-PD. In Proceedings of the European Conference on Optical Communication, Rome, Italy, 23–27 September 2018; pp. 1–3. [CrossRef]
64. Stojanovic, N.; Prodaniuc, C.; Zhang, L.; Wei, J. 210/225 Gbit/s PAM-6 transmission with BER bellow KP4-FEC/EFEC and at least 14 dB link budget. In Proceedings of the European Conference on Optical Communication, Rome, Italy, 23–27 September 2018; pp. 1–3. [CrossRef]
65. Masuda, A.; Yamamoto, S.; Taniguchi, H.; Nakamura, M.; Kisaka, Y. 255-Gbps PAM-8 transmission under 20-GHz bandwidth limitation using NL-MLSE based on volterra filter. In Proceedings of the Optical Fiber Communications Conference and Exhibition, San Diego, CA, USA, 3–7 March 2019; p. W4I.6.
66. Rahman, T.; Calabrò, S.; Stojanovic, N.; Zhang, L.; Wei, J.; Xie, C. LUT-assisted pre-compensation for 225 Gb/s/λ O-band transmission. In Proceedings of the European Conference on Optical Communication, Dublin, Ireland, 22–26 September 2019; pp. 1–3. [CrossRef]
67. Zhang, J.; Wang, K.; Wei, Y.; Zhao, L.; Zhou, W.; Xiao, J.; Liu, B.; Xin, X.; Zhao, F.; Dong, Z.; et al. 280 Gb/s IM/DD PS-PAM-8 Transmission Over 10 km SSMF at O-band For Optical Interconnects. In Proceedings of the Optical Fiber Communication Conference, San Diego, CA, USA, 8–12 March 2020; p. M4F.1.
68. Wang, K.; Zhang, J.; Wei, Y.; Zhao, L.; Zhou, W.; Zhao, M.; Xiao, J.; Pan, X.; Liu, B.; Xin, X.; et al. 100-Gbit/s/λ PAM-4 signal transmission over 80-km SSMF based on an 18-GHz EML at O-band. In Proceedings of the Optical Fiber Communication Conference, San Diego, CA, USA, 8–12 March 2020; p. Th1D.5.
69. Shindo, T.; Fujiwara, N.; Kanazawa, S.; Nada, M.; Yoshimatsu, T.; Kanda, A. 106 Gbit/s PAM4 60-km fibre-amplifierless transmission using SOA assisted extended reach EML (AXEL) with average output power of over 9 dBm. In Proceedings of the European Conference on Optical Communication, Dublin, Ireland, 22–26 September 2019; pp. 1–3. [CrossRef]
70. Zhong, K.; Zhou, X.; Huo, J.; Zhang, H.; Yuan, J.; Yang, Y.; Yu, C.; Lau, A.P.T.; Lu, C. Amplifier-Less Transmission of Single Channel 112Gbit/s PAM4 Signal Over 40km Using 25G EML and APD at O band. In Proceedings of the European Conference on Optical Communication, Gothenburg, Sweden, 17–21 September 2017; pp. 1–3. [CrossRef]
71. Chuang, C.; Liu, L.; Wei, C.; Liu, J.; Henrickson, L.; Huang, W.; Wang, C.; Chen, Y.; Chen, J. Convolutional Neural Network based Nonlinear Classifier for 112-Gbps High-speed Optical Link. In Proceedings of the Optical Fiber Communications Conference and Exposition, San Diego, CA, USA, 11–15 March 2018; p. W2A.43.
72. Huo, J.; Zhou, X.; Zhong, K.; Tu, J.; Yuan, J.; Guo, C.; Long, K.; Yu, C.; Lau, A.; Lu, C. Transmitter and receiver DSP for 112 Gbit/s PAM-4 amplifier-less transmissions using 25G-class EML and APD. *Opt. Express* **2018**, *26*, 22673–22686. [CrossRef] [PubMed]
73. Wang, W.; Zou, D.; Li, F. Digital pre-distortion enabled chirp-optimized C-band EML in 129 Gbit/s PAM-8 signal transmission for DCI-campus. *Opt. Commun.* **2020**, *464*, 125550. [CrossRef]
74. Wang, W.; Huang, Z.; Pan, B.; Li, H.; Li, G.; Tang, J.; Lu, Y. Demonstration of 214Gbps per lane IM/DD PAM-4 transmission using O-band 35GHz-class EML with advanced MLSE and KP4-FEC. In Proceedings of the Optical Fiber Communication Conference, San Diego, CA, USA, 8–12 March 2020; p. M4F.4.
75. Zhang, J.; Yu, J.; Zhao, L.; Wang, K.; Shi, J.; Li, X.; Kong, M.; Zhou, W.; Pan, X.; Liu, B.; et al. Demonstration of 260-Gb/s Single-Lane EML-Based PS-PAM-8 IM/DD for Datacenter Interconnects. In Proceedings of the Optical Fiber Communications Conference and Exhibition, San Diego, CA, USA, 3–7 March 2019; p. W4I.4.
76. Mardoyan, H.; Jorge, F.; Ozolins, O.; Estaran, J.; Udalcovs, A.; Konczykowska, A.; Riet, M.; Duval, B.; Nodjiadjim, V.; Dupuy, J.; et al. 204-GBaud On-Off Keying Transmitter for Inter-Data Center Communications. In Proceedings of the Optical Fiber Communication Conference Postdeadline Papers, San Diego, CA, USA, 11–15 March 2018; p. Th4A.4.
77. Ozolins, O.; Pang, X.; Udalcovs, A.; Schatz, R.; Westergren, U.; Rodrigo Navarro, J.; Kakkar, A.; Nordwall, F.; Engenhardt, K.; Chen, J.; et al. 100 Gbaud 4PAM Link for High Speed Optical Interconnects. In Proceedings of the European Conference on Optical Communication, Gothenburg, Sweden, 17–21 September 2017; pp. 1–3. [CrossRef]
78. Zhang, L.; Hong, X.; Pang, X.; Ozolins, O.; Udalcovs, A.; Schatz, R.; Guo, C.; Zhang, J.; Nordwall, F.; Engenhardt, K.; et al. Nonlinearity-aware 200 Gbit/s DMT transmission for C-band short-reach optical interconnects with a single packaged electro-absorption modulated laser. *Opt. Lett.* **2018**, *43*, 182–185. [CrossRef] [PubMed]
79. Li, M.; Wang, L.; Li, X.; Xiao, X.; Yu, S. Silicon intensity Mach–Zehnder modulator for single lane 100 Gb/s applications. *Photon. Res.* **2018**, *6*, 109–116. [CrossRef]
80. Chagnon, M.; Osman, M.; Poulin, M.; Latrasse, C.; Gagné, J.; Painchaud, Y.; Paquet, C.; Lessard, S.; Plant, D. Experimental study of 112 Gb/s short reach transmission employing PAM formats and SiP intensity modulator at 1.3 µm. *Opt. Express* **2014**, *22*, 21018–21036. [CrossRef] [PubMed]
81. Zhang, F.; Zhu, Y.; Yang, F.; Zhang, L.; Ruan, X.; Li, Y.; Chen, Z. Up to Single Lane 200G Optical Interconnects with Silicon Photonic Modulator. In Proceedings of the Optical Fiber Communications Conference and Exhibition, San Diego, CA, USA, 3–7 March 2019; p. Th4A.6.
82. Zhu, Y.; Zhang, F.; Yang, F.; Zhang, L.; Ruan, X.; Li, Y.; Chen, Z. Toward Single Lane 200G Optical Interconnects With Silicon Photonic Modulator. *IEEE J. Lightwave Technol.* **2020**, *38*, 67–74. [CrossRef]
83. Zhang, L.; Yang, F.; Ruan, X.; Li, Y.; Zhang, F. Single lane 176Gb/s Single Sideband PAM-4 Transmission over 400km with a Silicon Photonic Dual-drive Mach-Zehnder Modulator. In Proceedings of the Optical Fiber Communications Conference and Exhibition, San Diego, CA, USA, 8–12 March 2020; p. T3I.4.

84. Ming, H.; Zhang, L.; Yang, F.; Ruan, X.; Zhang, F. High-speed SSB transmission with a silicon MZM and a soft combined artificial neural network-based equalization. *Opt. Lett.* **2020**, *45*, 2066–2069. [CrossRef] [PubMed]
85. Samani, A.; El-Fiky, E.; Morsy-Osman, M.; Li, R.; Patel, D.; Hoang, T.; Jacques, M.; Chagnon, M.; Abadía, N.; Plant, D.V. Silicon Photonic Mach–Zehnder Modulator Architectures for on Chip PAM-4 Signal Generation. *IEEE J. Lightwave Technol.* **2019**, *37*, 2989–2999. [CrossRef]
86. Jacques, M.; Xing, Z.; Samani, A.; Li, X.; El-Fiky, E.; Alam, S.; Carpentier, O.; Koh, P.; Plant, D. Net 212.5 Gbit/s transmission in O-band with a SiP MZM, One driver and linear equalization. In Proceedings of the Optical Fiber Communications Conference and Exhibition, San Diego, CA, USA, 8–12 March 2020; p. Th4A.3.
87. Mardoyan, H.; Jorge, F.; Baeuerle, B.; Estaran, J.M.; Heni, W.; Konczykowska, A.; Bigo, S. 222-GBaud on-off keying transmitter using ultra-high-speed 2:1-selector and plasmonic modulator on silicon photonics. In Proceedings of the European Conference on Optical Communication, Dublin, Ireland, 22–26 September 2019; pp. 1–3. [CrossRef]
88. Zhang, H.; Li, M.; Zhang, Y.; Zhang, D.; Liao, Q.; He, J.; Hu, S.; Zhang, B.; Wang, L.; Xiao, X.; et al. 800 Gbit/s transmission over 1 km single-mode fiber using a four-channel silicon photonic transmitter. *Photon. Res.* **2020**, *8*, 1776–1782. [CrossRef]
89. Tong, Y.; Hu, Z.; Wu, X.; Liu, S.; Chang, L.; Netherton, A.; Chan, C.; Bowers, J.E.; Tsang, H. An Experimental Demonstration of 160-Gbit/s PAM-4 Using a Silicon Micro-Ring Modulator. *IEEE Photonics Technol. Lett.* **2019**, *32*, 125–128. [CrossRef]
90. Sun, J.; Kumar, R.; Sakib, M.; Driscoll, J.; Jayatilleka, H.; Rong, H. A 128 Gb/s PAM4 silicon microring modulator with integrated thermooptic resonance tuning. *IEEE J. Lightwave Technol.* **2018**, *36*, 110–115.
91. Xu, Y.; Li, F.; Kang, Z.; Huang, D.; Zhang, X.; Tam, H.-Y.; Wai, P.K.A. Hybrid Graphene-Silicon Based Polarization-Insensitive Electro-Absorption Modulator with High-Modulation Efficiency and Ultra-Broad Bandwidth. *Nanomaterials* **2019**, *9*, 157. [CrossRef] [PubMed]
92. Mecozzi, A.; Antonelli, C.; Shtaif, M. Kramers-Kronig receivers. *Adv. Opt. Photon.* **2019**, *11*, 480–517. [CrossRef]
93. Füllner, C.; Adib, M.M.H.; Wolf, S.; Kemal, J.N.; Freude, W.; Koos, C.; Randel, S. Complexity analysis of the Kramers-Kronig receiver. *IEEE J. Lightwave Technol.* **2019**, *37*, 4295–4307. [CrossRef]
94. Bo, T.; Kim, H. Kramers-Kronig receiver operable without digital upsampling. *Opt. Express* **2018**, *26*, 13810–13818. [CrossRef]
95. Chen, X.; Antonelli, C.; Chandrasekhar, S.; Raybon, G.; Mecozzi, A.; Shtaif, M.; Winzer, P. Kramers-Kronig Receivers for 100-km Datacenter Interconnects. *IEEE J. Lightwave Technol.* **2018**, *36*, 79–89. [CrossRef]
96. Li, Z.; Erkilinç, M.S.; Shi, K.; Sillekens, E.; Galdino, L.; Thomsen, B.C.; Bayvel, P.; Killey, R.I. 168 Gb/s/λ Direct-Detection 64-QAM SSB Nyquist-SCM Transmission over 80 km Uncompensated SSMF at 4.54 b/s/Hz net ISD using a Kramers-Kronig Receiver. In Proceedings of the European Conference on Optical Communication, Gothenburg, Sweden, 17–21 September 2017; pp. 1–3. [CrossRef]
97. Chen, X.; Antonelli, C.; Chandrasekhar, S.; Raybon, G.; Mecozzi, A.; Shtaif, M.; Winzer, P. 4× 240 Gb/s dense WDM and PDM Kramers-Kronig detection with 125-km SSMF transmission. In Proceedings of the European Conference on Optical Communication, Gothenburg, Sweden, 17–21 September 2017; pp. 1–3. [CrossRef]
98. Schuh, K.; Le, S.T.; Dischler, R.; Buchali, F. Transmission of 90 Gbd 32 QAM over 480 km of SSMF with Kramers-Kronig Detection. In Proceedings of the Optical Fiber Communications Conference and Exhibition, San Diego, CA, USA, 3–7 March 2019; p. Tu2B.3.
99. Shu, L.; Li, J.; Wan, Z.; Yu, Z.; Li, X.; Luo, M.; Fu, S.; Xu, K. Single-photodiode 112-Gbit/s 16-QAM transmission over 960-km SSMF enabled by Kramers-Kronig detection and sparse I/Q Volterra filter. *Opt. Express* **2018**, *26*, 24564–24576. [CrossRef]
100. Le, S.T.; Schuh, K.; Chagnon, M.; Buchali, F.; Buelow, H. 1.6 Tb/s Virtual-Carrier Assisted WDM Direct Detection Transmission Over 1200 km. *IEEE J. Lightwave Technol.* **2019**, *37*, 418–424. [CrossRef]
101. Hoang, T.M.; Zhuge, Q.; Xing, Z.; Sowailem, M.; Morsy-Osman, M.; Plant, D.V. Single Wavelength 480 Gb/s Direct Detection Transmission Over 80 km SSMF Enabled by Stokes Vector Receiver and Reduced-Complexity SSBI Cancellation. In Proceedings of the Optical Fiber Communication Conference, San Diego, CA, USA, 11–15 March 2018; p. W4E.7.
102. Che, D.; Chandrasekhar, S.; Chen, X.; Raybon, G.; Winzer, P.; Sun, C.; Shieh, W. Single-Channel Direct Detection Reception beyond 1 Tb/s. In Proceedings of the Optical Fiber Communication Conference, Postdeadline Papers, Anaheim, CA, USA, 20–24 March 2016; p. Th4B.7.
103. Pan, Y.; Yan, L.; Yi, A.; Jiang, L.; Pan, W.; Luo, B. Simultaneous demultiplexing of 2×PDM-PAM4 signals using simplified receiver. *Opt. Express* **2019**, *27*, 1869–1876. [CrossRef] [PubMed]
104. Liang, D.; Bowers, J. Recent Progress in Heterogeneous III-V-on-Silicon Photonic Integration. *Light Adv. Manuf.* **2021**, *2*. [CrossRef]
105. Ferrari, C.; Bolle, C.; Cappuzzo, M.A.; Keller, R.; Klemens, F.; Low, Y.; Basavanhally, N.; Papazian, A.R.; Pardo, F.; Earnshaw, M.P.; et al. Compact hybrid-integrated 400 Gbit/s WDM receiver for short-reach optical interconnect in datacenters. In Proceedings of the European Conference on Optical Communication, Cannes, France, 21–25 September 2014; pp. 1–3. [CrossRef]
106. Ghosh, S.; Suganuma, T.; Ishimura, S.; Nakano, Y.; Tanemura, T. Complete retrieval of multi-level Stokes vector signal by an InP-based photonic integrated circuit. *Opt. Express* **2019**, *27*, 36449–36458. [CrossRef] [PubMed]
107. Zhang, F.; Ruan, X.; Zhu, Y.; Chen, Z.; Qiu, X.; Yang, F.; Li, K.; Li, Y. Compact polarization diversity Kramers-Kronig coherent receiver on silicon chip. *Opt. Express* **2019**, *27*, 23654–23660. [CrossRef] [PubMed]
108. Estarán, J.; Usuga, M.A.; da Silva, E.P.; Piels, M.; Olmedo, M.I.; Zibar, D.; Monroy, I.T. Quaternary Polarization-Multiplexed Subsystem for High-Capacity IM/DD Optical Data Links. *IEEE J. Lightwave Technol.* **2015**, *33*, 1408–1416. [CrossRef]